CHALMERS

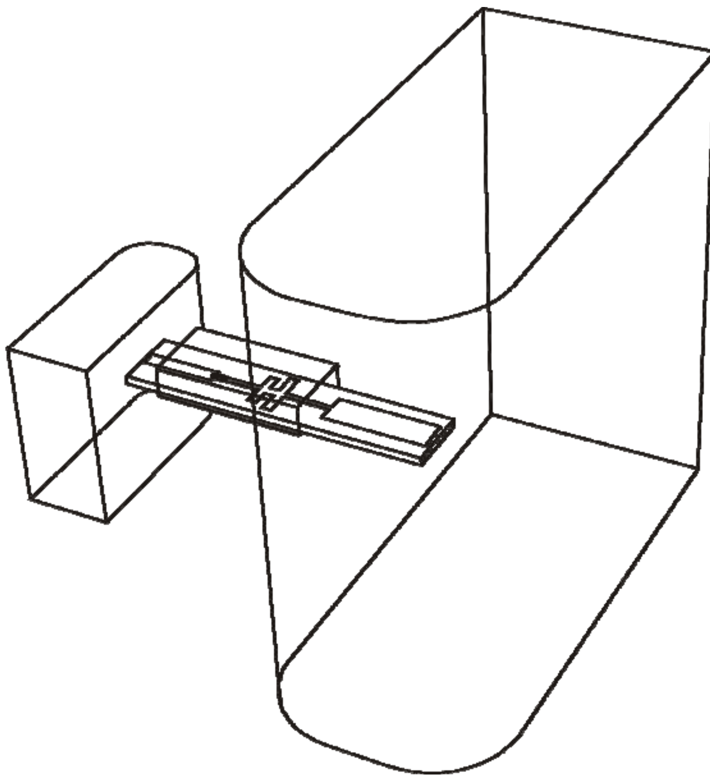

HBV diodes for THz applications

Design of a heterostructure barrier varactor frequency tripler for a 630 GHz output

Thesis for the degree of Master of Science in Wireless and Photonics Engineering

JOHANNA HANNING

Terahertz and Millimetre Wave Laboratory
Department of Microtechnology and Nanoscience
CHALMERS UNIVERSITY OF TECHNOLOGY
Göteborg, Sweden, 2011

Thesis for the degree of Master of Science
in Wireless and Photonics Engineering

HBV Diodes for THz Applications

Design of a Heterostructure Barrier Varactor Frequency Tripler for a 630 GHz Output

JOHANNA HANNING

Terahertz and Millimetre Wave Laboratory
Department of Microtechnology and Nanoscience
CHALMERS UNIVERSITY OF TECHNOLOGY
Göteborg, Sweden 2011

HBV Diodes for THz Applications
Design of a Heterostructure Barrier Varactor Frequency Tripler for a 630 GHz Output
JOHANNA HANNING

© JOHANNA HANNING, 2011

Terahertz and Millimetre Wave Laboratory
Department of Microtechnology and Nanoscience
Chalmers Univeristy of Technology
SE-412 96 Göteborg
Sweden
Telephone + 46 (0)31-772 1000

Cover:
Stylised circuit model, showing waveguide input and output, as well as MMIC circuit inside the waveguide channel.

This report is written in LaTeX

TeknologTryck
Göteborg, Sweden 2011

HBV Diodes for THz Applications
Design of a Heterostructure Barrier Varactor Frequency Tripler
for a 630 GHz Output
JOHANNA HANNING
Terahertz and Millimetre Wave Laboratory
Department of Microtechnology and Nanoscience
Chalmers University of Technology

Abstract

In this thesis a HBV tripler for an output frequency of 630 GHz is developed. The designed HBV is based on the InGaAs/InAlAs/AlAs epitaxially grown on InP material system and will be realised using a MMIC microstrip circuit inside a waveguide block. The doping and layer structure impact on the cut-off frequency is evaluated as well as the effects of self heating when choosing an appropriate structure. The circuit design in the complex topology is carried out through full electro-magnetic field FEM simulations in HFSS complemented by harmonic balance simulation and optimisation in ADS. The finished multiplier simulations indicate an output power above 1 mW for an input power of 40 mW, and a relative halfpower bandwidth of 9 % at 630 GHz. Limiting factors are self heating, limited available input power, and fabrication tolerances for mesa size and substrate dimensions.

Keywords: HBV, THz, frequency multipliers, tripler, terahertz sources, varactors, harmonic generation, submm, submillimeter

Acknowledgements

This thesis work would not have been possible without the excellent guidance from my two supervisors, professor Jan Stake and Dr. Tomas Bryllert. I would especially like to thank professor Stake for believing in me, and for giving me the opportunity to work at the Terahertz and Millimetre Wave Laboratory, and Dr. Bryllert and Dr. Josip Vukusic for their help with simulation models. I would also like to thank the entire staff at Terahertz and Millimetre Wave Laboratory, for their friendship and providing an inspiring and pleasant research environment. Who knew you were such excellent sailors? Finally, I would like to thank Vetenskapsrådet, VR for funding this research.

Contents

Abstract i

Acknowledgements iii

Acronyms and abbreviations vii

1 Introduction 1
- 1.1 Terahertz sources . . . 1
- 1.2 Heterostructure Barrier Varactor frequency multipliers . . . 2
- 1.3 Scope . . . 3

2 Theory 5
- 2.1 Varactor . . . 5
  - 2.1.1 Varactor efficiency . . . 5
  - 2.1.2 Varactor figures-of-merit . . . 6
- 2.2 Heterostructure Barrier Varactor . . . 7
  - 2.2.1 HBV physics - capacitance . . . 7
  - 2.2.2 HBV physics - conduction current . . . 9
  - 2.2.3 HBV model . . . 9
  - 2.2.4 Series resistance and parasitics . . . 11
  - 2.2.5 Electro-thermal model . . . 12
  - 2.2.6 HBV materials . . . 12
- 2.3 HBV impedance matching . . . 14
- 2.4 Wave guiding structures . . . 15

3 Method 17
- 3.1 Material design . . . 17
- 3.2 Diode design . . . 17
  - 3.2.1 Self-heating simulations . . . 18
  - 3.2.2 Electro-thermal simulations . . . 19
- 3.3 Circuit design . . . 19
  - 3.3.1 Realisation of planar diode structure . . . 20
  - 3.3.2 Input and output probe design . . . 21
  - 3.3.3 Input matching circuit design . . . 21

4 Results 25
- 4.1 Material investigation . . . 25
- 4.2 Diode simulation results . . . 27
- 4.3 Circuit simulation results . . . 27

4.3.1 Waveguide channel and substrate dimensions 28
4.3.2 Planar diode structure 28
4.3.3 Input and output probes 28
4.3.4 Input matching circuit 30
4.4 Final tripler circuit design results 30

5 Discussion and conclusion **37**
5.1 Discussion 37
5.2 Conclusion 38

References **39**

Appendix **43**

A Paper A **43**

Acronyms and abbreviations

ADS	Agilent technologies Advanced design system simulation software
FEM	Finite element method
HFSS	Ansoft HFSS^{TM} numerical software
HBV	Heterostructure barrier varactor
LO	Local oscillator
MMIC	Microwave monolithic integrated circuit
QCL	Quantum cascade laser
RTD	Resonant tunneling diode
RL	Return loss
THz	Terahertz

Chapter 1

Introduction

Terahertz (THz) waves have been of much interest in recent years. Early research on THz technology was driven by astronomers and chemists for the possibility to observe molecular signatures of gases at a distance. But lately the interest in terahertz has expanded to include medical and safety applications [1,2].

Terahertz refers to frequencies in the electromagnetic spectrum between high frequency microwaves and long wavelength infrared radiation in the optical end of the spectrum [1]. The frequency range covered by THz normally includes 0.1 - 10 THz, although there is no stated convention. This frequency range is often referred to as the THz gap due to the rapid decrease of output power for signal sources in this range. From an optical point of view the low photon energy due to the long wavelength introduces a challenge in producing solid-state sources and detectors. On the other hand electronic components for THz applications are limited by electron mobility, and the high precision processing needed for the delicate circuits related to the high frequency with corresponding short wavelengths.

1.1 Terahertz sources

Terahertz sources are needed in heterodyne receivers for radio astronomy, as well as in imaging and radar applications, and in spectroscopy. The fundamental LO sources available today in the THz regime are scarce, and usually unpractical, bulky, expensive or need cryogenical cooling. The quantum cascade laser (QCL) for example, emits radiation above 1 THz [3], but it is a narrowband device and needs cooling to cryogenic temperatures. Other examples of fundamental sources are the p-Ge laser, which works at 4 K, the free-electron laser which requires an electron accelerator, and the resonant tunneling diode (RTD) which provides a limited power at terahertz frequencies [3].

Another approach to produce terahertz waves is by frequency conversion. The unitraveling carrier photo diode is a solid-state electronic device which generates terahertz frequencies by means of photomixing. For this purpose two laser diodes are needed, and the output power decreases rapidly as the frequency moves up towards 1 THz [3].

Therefore the most commonly used and efficient solution for LO signal sources today is frequency upconversion through multiplication by non-linear

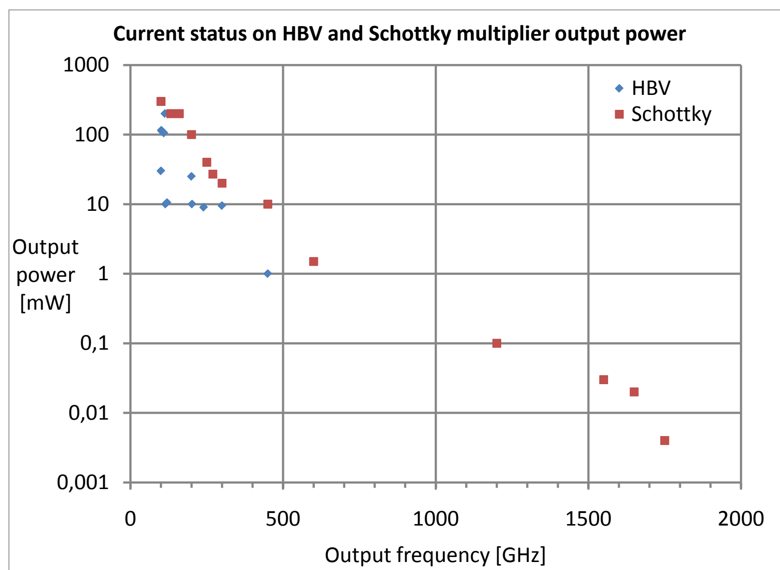

Figure 1.1: Current status on output power for single diode HBV frequency multipliers and Schottky diode frequency multiplier chains [4, 8–10].

semiconductor devices [1]. Multiplier sources providing power at close to 2 THz have been published [4]. Today most frequency multiplier circuits are realised using Schottky diodes [1]. Due to their high performance, balanced Schottky doublers have become standard as multiplier sources, and planar Schottky diode multipliers for the THz frequency range have been demonstrated [5].

An alternative to the Schottky diode is the Heterostructure Barrier Varactor (HBV), see Figure 1.1. Ever since the invention in 1989, the HBV diode has been promising for frequency multiplication to THz frequencies [6]. Today HBV diodes are used as high power multipliers for frequencies up to and above 200 GHz [7].

1.2 Heterostructure Barrier Varactor frequency multipliers

The HBV consists of a wide bandgap semiconductor barrier spaced between two narrow bandgap, equally doped, semiconductor modulation layers. The C-V curve is symmetric, while the I-V curve is anti-symmetric, see Figure 1.2, and these properties cause the HBV to only generate odd harmonics. Thereby, when used as a frequency tripler, there is only need for circuit matching at the in- and output frequencies, and no idler matching is needed. In addition, there is no need for DC-biasing, which together with the matching requirements enables a simple and compact circuit design.

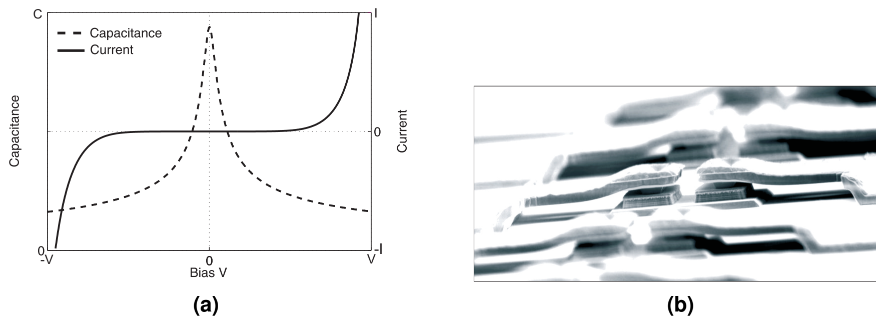

Figure 1.2: (a) C-V and I-V curve for a HBV diode. C-V is symmetric while I-V is antisymmetric. (b) SEM image of a two-mesa HBV diode with a total of six barriers, and gold air bridges.

Another advantage is that the sandwich structure of the HBV allows stacking of several diodes for better power handling capability, and at the same time diode miniaturisation is prevented [10]. In recent years the focus in research has been on high power HBV, and the highest output frequency published for HBV diode based multipliers is 450 GHz [11]. The purpose of this thesis work is to present a HBV frequency tripler with an output frequency of 630 GHz that will use an in-house multiplier pumping source at 210 GHz. In this frequency region there is a window in the atmospheric absorption spectrum [2], making it interesting for THz imaging applications, for example.

1.3 Scope

In this thesis a HBV tripler for an output frequency of 630 GHz is developed. The designed HBV is based on the InGaAs/InAlAs/AlAs epitaxially grown on InP material system and will be realised using a microwave monolithic (MMIC) microstrip circuit inside a waveguide block. The doping and layer structure impact on the cut-off frequency is evaluated as well as the effects of self heating when choosing an appropriate diode structure. The circuit design in the complex topology is carried out through full electro-magnetic field FEM simulations in Ansoft HFSS (HFSS) complemented by harmonic balance simulation and optimisation in Agilent Technologies Advanced Design System (ADS). The simulated results of the finished circuit design is presented in the end of this report.

In the next chapter the necessary theory behind HBV based frequency multipliers is presented. Then, in the third chapter, the design methodology is explained, and in the fourth chapter the design results are presented. The report ends with a chapter on discussion and concluding remarks.

Chapter 2

Theory

This chapter deals with the necessary theory behind designing a HBV frequency tripler. The heterostructure barrier varactor is a special case of a symmetric varactor, why this chapter starts with the necessary theory of varactors used in designing the frequency multiplier. The chapter then moves on to describing the theory of HBVs and of HBV multiplier circuit design.

2.1 Varactor

The name varactor comes from variable reactance, but it generally refers to a nonlinear capacitance. The varactor properties makes it suitable for applications involving conversion of power from one frequency to another, such as frequency multiplication, frequency division and mixing [12]. In the most simplified equivalent circuit, the varactor is represented by a voltage dependent capacitance, connected in series with a resistance, see Figure 2.1.

Figure 2.1: General equivalent circuit of a varactor [12, 13].

2.1.1 Varactor efficiency

Ideally the varactor has zero series resistance, i.e. no losses. Then the power conversion, for a lossless nonlinear reactance excited at two different frequencies,

can be described by the Manley-Rowe formulas [14]

$$\sum_{m=1}^{\infty}\sum_{n=-\infty}^{\infty}\frac{mP_{\mathrm{m,n}}}{m\omega_{\mathrm{s}}+n\omega_{\mathrm{p}}}=0 \tag{2.1a}$$

$$\sum_{m=-\infty}^{\infty}\sum_{n=1}^{\infty}\frac{nP_{\mathrm{m,n}}}{m\omega_{\mathrm{s}}+n\omega_{\mathrm{p}}}=0. \tag{2.1b}$$

Where ω_{p} and ω_{s} are the pumping and signal frequencies respectively, n and m are the order of the harmonic and $P_{\mathrm{m,n}}$ is the power at the frequency $m\omega_s+n\omega_p$. For a frequency multiplier $m=0$, reducing the Manley-Rowe formulas to

$$\sum_{n=1}^{\infty}P_{\mathrm{n}}=0 \tag{2.2}$$

where P_{n} is the power at $n\omega_{\mathrm{p}}$. Thus predicting 100% efficiency for an ideal varactor multiplier circuit.

Not to be confused with the varactor is the varistor. Varistors are based on a nonlinear resistance, and when used in multipliers the maximum conversion efficiency of varistors is $1/n^2$ for the nth harmonic [15]. In other words, the advantage of a multiplier circuit based on a varactor over a passive varistor is great.

However, a real varactor is not lossless, and especially at high frequencies does the series resistance limit the efficiency [12].

2.1.2 Varactor figures-of-merit

In order to predict the performance of a varactor, one can use the varactor figure-of-merit. An important and widely used figure-of-merit is the dynamic cut-off frequency. From the simple equivalent circuit in Figure 2.1, the varactor cut-off frequency is defined as

$$f_{\mathrm{c}}=\frac{1}{2\pi R_{\mathrm{S}}C_{\mathrm{max}}} \tag{2.3}$$

The differential capacitance in (2.3) can for convenience be replaced by the differential elastance

$$S(V)=\frac{dV}{dQ}=\frac{1}{C(V)}. \tag{2.4}$$

For a symmetric varactor, the elastance is uniquely defined from S_{min} to S_{max} [16, 17], and the cut-off frequency is defined as

$$f_{\mathrm{c}}=\frac{S_{\mathrm{max}}-S_{\mathrm{min}}}{2\pi R_{\mathrm{S}}}. \tag{2.5}$$

Thus to increase the cut-off frequency it is necessary to increase the difference $S_{\mathrm{max}}-S_{\mathrm{min}}$ and decrease the series resistance R_{S}.

Another figure of merit is the maximum conversion efficiency. For the HBV there is an empirical expression for the estimation of the maximum conversion efficiency

$$\eta\approx\frac{100}{1+\alpha\left(\frac{f_{\mathrm{p}}}{f_{\mathrm{c}}}\right)^{\beta}}\% \tag{2.6}$$

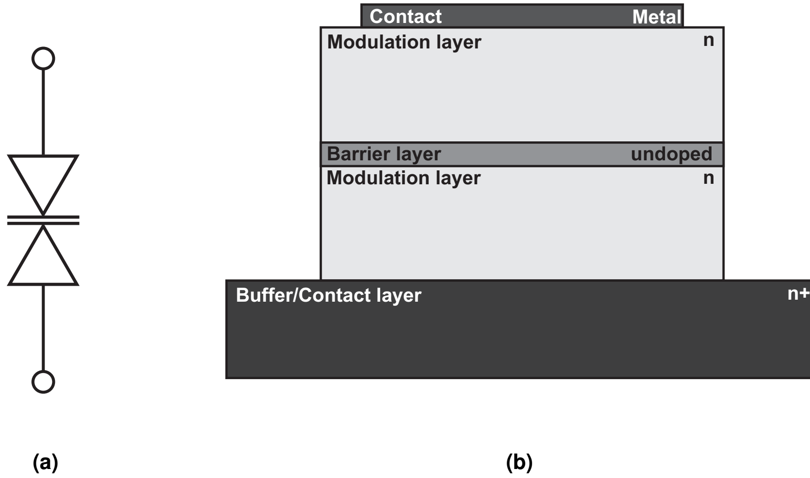

Figure 2.2: (a) HBV circuit schematic symbol. (b) Structure of a single barrier HBV showing the layer structure and the doping profile.

where f_p is the pumping frequency, f_c the cutoff frequency, $\alpha = 200$ and $\beta = 1.5$ [18].

2.2 Heterostructure Barrier Varactor

The heterostructure barrier varactor is a symmetric diode and consists of a wide bandgap barrier material sandwiched in between two moderately n-doped modulation layers, see Figure 2.2. There are many advantages with the symmetric structure. For instance it is easy to series connect several diodes simply by stacking them on top of each other. Another advantage is the symmetrical C-V characteristic caused by the symmetric structure, that cause the HBV to only generate odd harmonics, $f_{2\mathrm{n}+1} = (2n+1)f_\mathrm{p}$, $n \in \mathbb{N}$.

Recent HBV diodes have a planar structure, whereas the early HBV diodes were whisker contacted. In the planar structure usually two or more mesas are connected in series, each mesa containing one or more barrier layers surrounded by two modulation layers. The mesas are then connected with each other through a highly doped conducting layer, and each mesa is contacted on top using air-bridges.

2.2.1 HBV physics - capacitance

The depletion of electrons in the modulation layer when a voltage is applied over the HBV gives rise to the voltage dependent non-linear capacitance, see Figures 2.2b-2.4. One can almost think of the HBV as a parallel plate capacitor where the distance between the plates change with the applied voltage. The maximum capacitance, i.e. minimum elastance, occur at zero bias when the distance between the "parallel plates" is minimum, determined by the barrier b

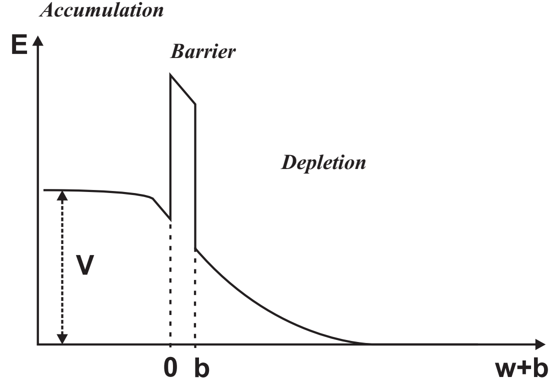

Figure 2.3: Conduction band diagram of a biased HBV.

and spacer s widths, and the Debye length L_{D} of the material

$$S_{\min} = \frac{N}{A}\left(\frac{b}{\varepsilon_{\mathrm{b}}} + \frac{2s}{\varepsilon_{\mathrm{d}}} + \frac{2L_{\mathrm{D}}}{\varepsilon_{\mathrm{d}}}\right) \tag{2.7}$$

$$L_{\mathrm{D}} = \sqrt{\frac{kT\varepsilon_{\mathrm{d}}}{q^2 N_{\mathrm{D}}}}, \tag{2.8}$$

in which N is the number of barriers and A the HBV area [18].

Conversely, the maximum elastance depends on the maximum distance, i.e. the maximum depletion width of electrons in the modulation layers $w_{\max}$

$$S_{\max} = \frac{N}{A}\left(\frac{b}{\varepsilon_{\mathrm{b}}} + \frac{2s}{\varepsilon_{\mathrm{d}}} + \frac{w_{\max}}{\varepsilon_{\mathrm{d}}}\right). \tag{2.9}$$

There are three governing effects that limits the maximum depletion width, impact ionisation, current saturation, and depletion layer punch through [18]. The impact ionisation occurs for large electric fields, and results in break down of the device. The maximum depletion width is directly proportional to the maximum field, $E_{\mathrm{d,max}}$

$$w_{\max} = \frac{\varepsilon_{\mathrm{d}} E_{\mathrm{d,max}}}{q N_{\mathrm{d}}}. \tag{2.10}$$

The current saturation, on the other hand, depend on the maximum velocity $v_{\max}$ of the carriers in the modulation layer, which limits how far they can travel during a quarter pump cycle

$$w_{\max} = \frac{v_{\max}}{8 f_{\mathrm{p}}}. \tag{2.11}$$

And the depletion layer punch through is related to the actual width of the modulation layer width, l

$$w_{\max} = l. \tag{2.12}$$

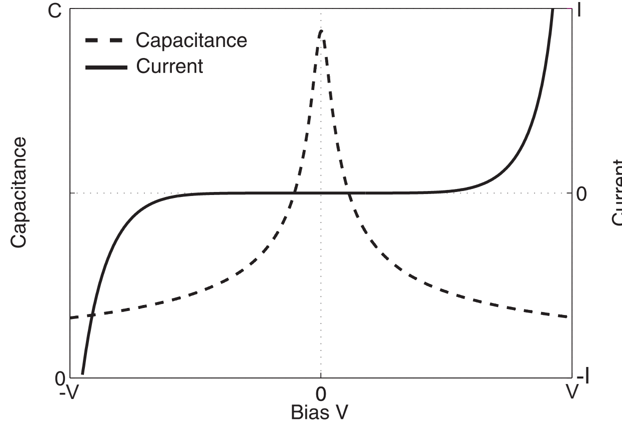

Figure 2.4: Typical C-V and I-V curves for a HBV.

2.2.2 HBV physics - conduction current

The characteristic I-V curve for the HBV diode, see Figure 2.4, derives from carrier transport through the barrier material. There are two main transport mechanisms governing the current, thermionic emission over the potential barrier, and quantum-mechanical tunneling through the barrier. For thermionic emission, only carriers with an energy higher than the barrier potential will transport over the barrier, see Figure 2.5. A simplified expression of the thermionic-emission current for positive bias voltage is given by the Richardson-Dushman equation

$$J = A^{*}T^{2}e^{-\frac{q\phi_{\mathrm{B}}}{kT}} \tag{2.13}$$

where ϕ_{B} is the effective barrier height. A^{*} is the Richardson constant

$$A^{*} \equiv \frac{4\pi q m^{*} k^{2}}{h^{3}} \tag{2.14}$$

which can be modified to include the tunneling current [19]. Equation (2.13) is valid under the assumption the the barrier thickness is smaller than the mean free path.

Furthermore, an applied voltage will decrease the effective barrier height, allowing more electrons to transport. Consequently, the conduction current through the barrier consisting of thermionic emission and tunneling depend on several factors such as the barrier thickness, barrier height, temperature, and applied voltage. And as the effective barrier height decrease for thicker barriers and increased applied voltages, as well as for high temperatures, the effect of thermionic emission on the conduction current increase. Whereas for smaller voltages and thinner barriers, the tunneling current through the barrier is dominating [20, 21].

2.2.3 HBV model

In order to design a HBV, accurate models for simulations are necessary. The quasi-empirical Chalmers HBV model has been developed for the purpose of

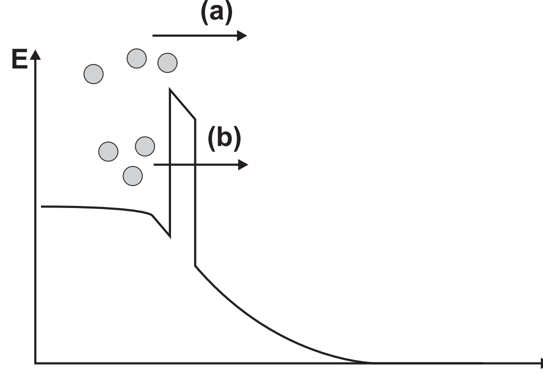

Figure 2.5: Electron transport through (a) thermionic emission over the barrier, and (b) tunneling through the barrier.

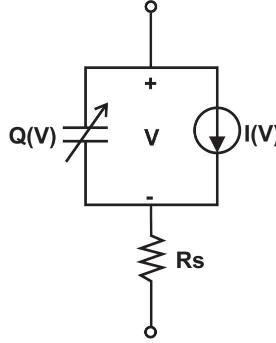

Figure 2.6: Equivalent circuit of a HBV, in which the conduction current through the HBV is modeled as a current source in parallel with the capacitance.

harmonic balance simulations and modeling of the non-linear capacitance [18]. The model is valid under the assumption of sufficiently low conduction current through the HBV so that the HBV works in varactor mode. The voltage across the capacitance in the HBV, and the corresponding displacement current can then be expressed as

$$\begin{aligned} V(Q) = N\Big\{ \frac{bQ}{\varepsilon_{\mathrm{b}}A} + 2\frac{sQ}{\varepsilon_{\mathrm{d}}A} + \mathrm{Sign}(Q)\cdot\Big(\frac{Q^2}{2qN_{\mathrm{d}}\varepsilon_{\mathrm{d}}A^2} + \\ + \frac{4k_{\mathrm{B}}T}{q}\Big(1-\exp\Big[-\frac{|Q|}{2L_{\mathrm{D}}AqN_{\mathrm{d}}}\Big]\Big)\Big)\Big\} \end{aligned} \tag{2.15}$$

$$i(t) = \frac{\partial Q}{\partial t} \tag{2.16}$$

where N is the number of barriers, b and s are the barrier and spacer layers, and A is the area of the HBV. The corresponding equivalent circuit if the model is shown in Figure 2.6.

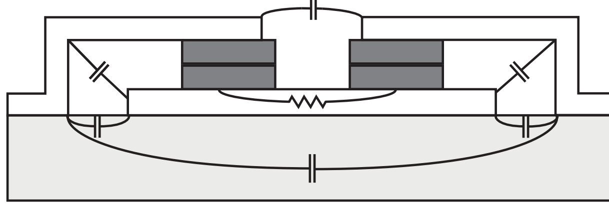

Figure 2.7: Illustration of parasitics in a planar HBV structure.

2.2.4 Series resistance and parasitics

The voltage dependent series resistance of a HBV diode can be approximated to a constant resistance which is the sum of several resistance elements

$$R_{\mathrm{S}} = R_{\mathrm{active}} + R_{\mathrm{spread,buff}} + R_{\mathrm{contact}}. \tag{2.17}$$

The resistance in the epi-layers is estimated by

$$R_{\mathrm{active}} = \sum_{n} \frac{l_{\mathrm{n}}}{\mu_{\mathrm{n}} N_{\mathrm{n}} q A} \tag{2.18}$$

where n is the layer number, l_{n} the layer thickness, μ_{n} the mobility of the layer material, N_{n} the doping of the layer material, and A is the mesa area. By approximating the resistance in the active layers as constant, a worst case scenario is assumed. The spreading resistance between two mesas or a mesa and contact in a single mesa diode is

$$R_{\mathrm{spread,buff}} = \frac{l_{\mathrm{buff}}}{\mu_{\mathrm{buff}} N_{\mathrm{buff}} q A_{\mathrm{buff}}} \tag{2.19}$$

where A_{buff} is the cross section area in the buffer layer. The ohmic contact resistance of an even number mesa diode is

$$R_{\mathrm{contact}} = N_{\mathrm{m}} \frac{r_{\mathrm{c}}}{A} \tag{2.20}$$

where N_{m} is the number of mesas and $r_{\mathrm{c}} = 100\ \Omega\text{-}\mu\mathrm{m}^2$.

The mobility is doping dependent and can be estimated using the low-field mobility model presented in [22]

$$\mu_{\mathrm{LF}}(N,T) = \mu_{\mathrm{min}} + \frac{\mu_{\mathrm{max}}(T_0)(T_0/T)^{\theta_1} - \mu_{\mathrm{min}}}{1 + \left(\frac{N}{N_{\mathrm{ref}}(T_0)(T/T_0)^{\theta_2}}\right)^{\lambda}} \tag{2.21}$$

$T_0 = 300$ K, and μ_{min}, $\mu_{\mathrm{max}}(T_0)$, $N_{\mathrm{ref}}(T_0)$, θ_1, θ_2 and λ are material specific constants listed in [22].

In addition to the series resistance, there are reactive parasitics that can degrade the performance of the HBV multiplier. In reducing parasitics trade-offs must be made, for example the stray capacitance between mesas versus the spreading resistance in the buffer layer between the two mesas, see Figure 2.7.

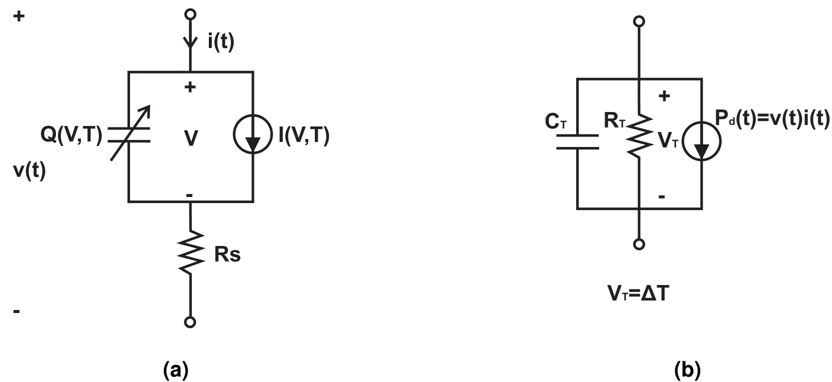

Figure 2.8: Electro thermal model of a HBV [23]

2.2.5 Electro-thermal model

Heating is an important factor to take into consideration when designing the diode, as it degrades the performance [24]. An electro-thermal HBV model for harmonic simulations is presented by Invarsson et al. (2005) [23]. The voltage, V_{T} over a thermal resistance R_{T}, is equivalent to the temperature rise ΔT in the diode, and the thermal capacitance C_{T} represents the thermal storage of the diode in this model, see Figure 2.8. The thermal and electrical models are linked via the applied time-dependent current and voltage, $i(t)$ and $v(t)$, through the diode, which are the factors of a time varying power source $P_{\mathrm{d}}(t)$ in the electro-thermal equivalent circuit [23].

2.2.6 HBV materials

The early HBV diodes were based on the epitaxially grown GaAs/AlGaAs/AlAs on GaAs substrate material system. The advantages of this material are the good thermal and electrical properties of GaAs as substrate material, as well as it being a well known material from a processing perspective. The drawbacks are the limited electron mobility and, more importantly, the small relative potential barrier height, see Figure 2.9, which cause large conduction current in the HBV.

At the present time most HBV are realised using the epitaxial InGaAs/InAlAs on InP material system, see Figure 2.9. The epitaxial layers can be designed and processed with high precision, using e.g. molecular beam epitaxy (MBE). The advantage of this material is the high relative barrier height and the high mobility of electrons in InGaAs. The drawbacks are the poor thermal conductivity of especially InGaAs which cause self heating problems for smaller HBV diodes [26], and the high relative permittivity of InP, see Table 2.1. For the InGaAs on InP material system theoretical research on HBV layer configurations, where an undoped high band gap semiconductor (barrier) is layered in between two moderately n-doped low band gap semiconductors (modulation layers), suggests that a material system of InAlAs/InGaAs has superior properties in regards to leakage current than a AlGaAs/GaAs system. In both cases a thin layer of AlAs is included in the middle of the barrier, and

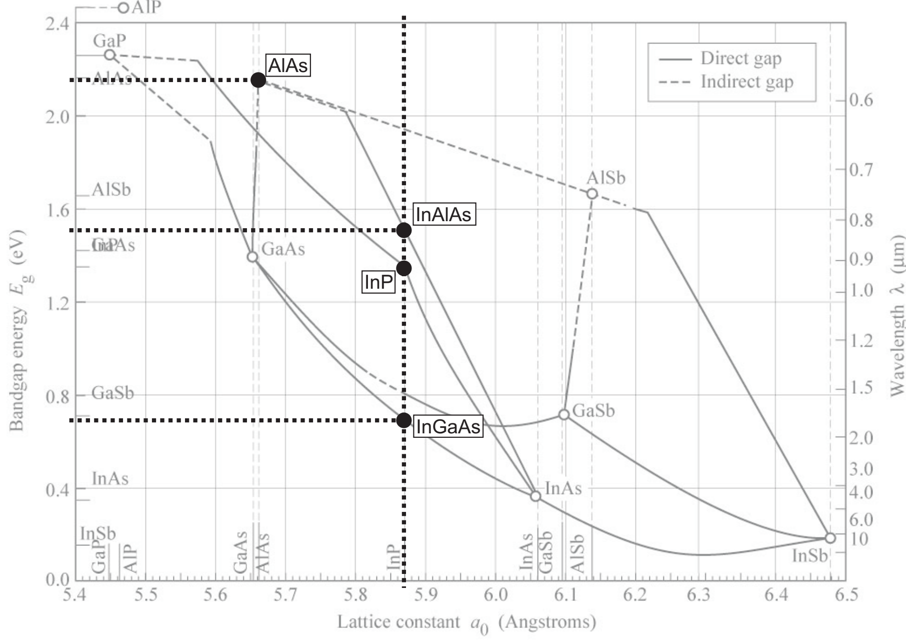

Figure 2.9: Energy and lattice constant for some III-V semiconductors at room temperature [25], featuring lattice matched InGaAs, InAlAs and InP. The concentration of the lattice matched materials are $In_{0.47}Ga_{0.53}As$ and $In_{0.48}Al_{0.52}As$. AlAs is mismatched to InP.

for InAlAs/InGaAs the theoretical optimum barrier layer configuration is 8 nm $In_{0.52}Al_{0.48}As$, 3 nm AlAs, and another 8 nm $In_{0.52}Al_{0.48}As$ [20]. The thickness of the high bandgap AlAs layer is limited, since it is strained to match the $In_{0.52}Al_{0.48}As$ lattice constant.

Table 2.1: Material properties of different HBV materials [27]

Property	**InP**	$\mathbf{In_{0.53}Ga_{0.47}As}$	**GaAs**	**InAs**
Relative permittivity ε_r	12.5	13.9	12.9	15.15
Thermal conductivity [W/cm-K]	0.68	0.05	0.55	0.27
Electron mobility [cm^2/V-s]	≤ 5400	$\leq 12 \cdot 10^3$	≤ 8500	$\leq 4 \cdot 10^4$
Energy bandgap [eV]	1.344	0.74	1.424	0.354

The barrier thickness for InGaAs/InAlAs/AlAs HBV diodes has been further optimised experimentally by Emadi et al. (2007) [21]. The optimum total barrier thickness lies between 10 and 14 nm for maximum breakdown voltage, and depends on the applied bias voltage and the operating temperature. Other material properties such as the doping and thickness of the modulation layer can be optimised through maximising the cut-off frequency (2.5). An example of a HBV material can be seen in Table 2.2.

There exist attempts to create HBV diodes in other materials, such as Si, GaN, and InAs [28–30]. However Si, e.g. suffers from low electron mobility and may not be suited for THz frequency multiplication. Resent results suggest that

Table 2.2: HBV active layer material specification.

Layer	**Material**	**Thickness [Å]**	**Doping [cm^{-3}]**	**Comment**
1	$In_{0.53}Ga_{0.47}As$	2,500	10^{17}	Modulation
2	$In_{0.53}Ga_{0.47}As$	50	Undoped	Spacer
3	$In_{0.52}Al_{0.48}As$	50	Undoped	Barrier
4	AlAs	30	Undoped	Barrier
5	$In_{0.52}Al_{0.48}As$	50	Undoped	Barrier
6	$In_{0.53}Ga_{0.47}As$	50	Undoped	Spacer
7-18	... 2 × Layers 1 - 6 ...			
19	$In_{0.53}Ga_{0.47}As$	2,500	10^{17}	Modulation

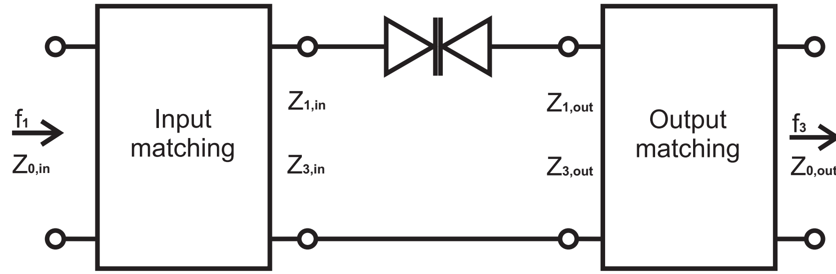

Figure 2.10: Two-port representation of a HBV diode with impedance matching networks for tripler operation.

bonding the epitaxial InGaAs/InAlAs/AlAs epi-layers to a Si substrate may improve the HBV characteristics further due to the advantages of Si technology and superior substrate properties [31].

2.3 HBV impedance matching

Since the HBV diode only generates odd harmonics of the input frequency, there is only need for matching at the in and output frequencies when used in a frequency tripler. The impedance matching circuit should be designed to match the fundamental frequency at the input of the diode, while reflecting all power from the diode at the third harmonic. And at the output the opposite case, match the optimum embedding impedance at the third harmonic, while reflecting all power from the fundamental frequency signal.

For pump frequency f_{p} an indication of the optimal matching impedances is given by

$$\frac{Z_{\mathrm{c},1}}{R_{\mathrm{S}}} = 1 + j \cdot \frac{S_{\min}}{R_{\mathrm{S}}\omega_{\mathrm{p}}} + \frac{f_{\mathrm{c}}}{f_{\mathrm{p}}}\left(A_1 + jB_1 - \rho_{\mathrm{d}}\varepsilon_{\mathrm{d}}\omega_{\mathrm{p}}(C_1 + jD_1)\right) \tag{2.22a}$$

$$\frac{Z_{\mathrm{c},3}}{R_{\mathrm{S}}} = 1 + j \cdot \frac{S_{\min}}{3R_{\mathrm{S}}\omega_{\mathrm{p}}} + \frac{f_{\mathrm{c}}}{f_{\mathrm{p}}}\left(\frac{A_3 + jB_3}{3} - \rho_{\mathrm{d}}\varepsilon_{\mathrm{d}}\omega_{\mathrm{p}}(C_3 + jD_3)\right) \tag{2.22b}$$

where the constants A_1 - D_3, are extracted fitting parameters [18].

Figures of merits for the matching network are the conversion efficiency, the resulting bandwidth and the return loss. In which the conversion efficiency at a given pump frequency is defined as

$$\eta = \frac{P_{\text{out}}}{P_{\text{in}}}. \tag{2.23}$$

Moreover the return loss at the circuit input is [32]

$$RL = -20\log\rho \tag{2.24}$$

where the reflection constant ρ is the absolute value of Γ_{in}

$$\Gamma_{\text{in}} = \frac{Z_{\text{in}} - Z_0}{Z_{\text{in}} + Z_0} = \rho e^{j\theta}. \tag{2.25}$$

Γ_{in} can be calculated from the large signal input impedance

$$Z_{\text{in}} = \frac{V_{\text{in}}}{I_{\text{in}}}. \tag{2.26}$$

2.4 Wave guiding structures

In recent years, the most common way to realise a HBV multiplier circuit is by inserting a microstrip circuit with matching components in a waveguide block, using rectangular waveguides as in- and output of the circuit. The electromagnetic waves are then coupled to the microstrip using E-probes.

To realise the multiplier a planar HBV can be used as a discrete diode, which is flip chip mounted on to a transmission line circuit, for example microstrip or coplanar waveguide. For higher frequencies the placement of the flip chipped diode becomes more critical, due to the shorter wavelengths, and the reliability and broadband performance may be compromised, thus a HBV realised in a MMIC may be more beneficial [33].

The high frequencies put constraints on the substrate thickness. Limiting factors of the thickness are thermal resistance, propagation losses, the fragility of the substrate, impedance line width concerns, and waveguide mode propagation in the substrate [33]. The last constraint is of major concern for the design of the MMIC HBV, since the substrate material, InP, has a high relative permittivity.

Consequently the substrate must be thinned down, which will make it more brittle and reduce the maximum characteristic impedance of the circuit lines for microstrip. Another option is to use suspended membrane technology, which is widely used in high frequency GaAs circuits. However, because of the fore mentioned problems for InP and because the InP has to be epitaxially grown on a substrate, and doped with Fe atoms to become semi-insulating, this may not be a suitable solution.

Chapter 3

Method

This chapter describes the design process of the HBV frequency tripler. There are several design steps involved, an investigation of the material design, diode structure and design for maximum conversion efficiency and low self-heating, and finally circuit simulation and optimisation using harmonic balance. Overall design goals are a frequency tripler with a 10 % bandwidth output around a center frequency of 630 GHz, with maximised efficiency and return loss, for a 20 mW input power at an input frequency of 210 GHz.

3.1 Material design

In order to optimise the diode material, an investigation of the epi-layer structure and the material properties is performed. A high cutoff frequency is crucial for the HBV performance at high frequency (2.5). Hence the cut-off frequency is calculated using equations (2.7) and (2.9) for the elastance, and equations (2.17)-(2.20) for the series resistance, with the mobility from (2.21), for different parameter variations using Matlab. The effect of current saturation and impact ionisation, as well as depletion layer punch through on the the maximum depletion width $w_{\max}$ has to be considered when calculating the cut-off frequency for different doping levels. An electron drift velocity in InGaAs of $3 \cdot 10^7$ cm/s [34] is used in the analysis. By varying the modulation layer doping level, the number of barriers, and the modulation layer thickness their respective optimum values for a maximised cut-off frequency can be decided.

3.2 Diode design

In choosing the shape of the HBV diode taking the effects of self heating into account is crucial due to the poor thermal conductivity of InGaAs. Using heat transfer FEM simulations combined with ADS harmonic balance simulations the heating in the diode active region and the conversion efficiency is estimated for different diode shapes. The efficiency and optimum impedances are determined by shape, size, and number of barriers and mesas. Hence one- and two mesa diodes are investigated as well as a two- and a three barrier material, with modulation layer thickness and doping level from the previous material analysis.

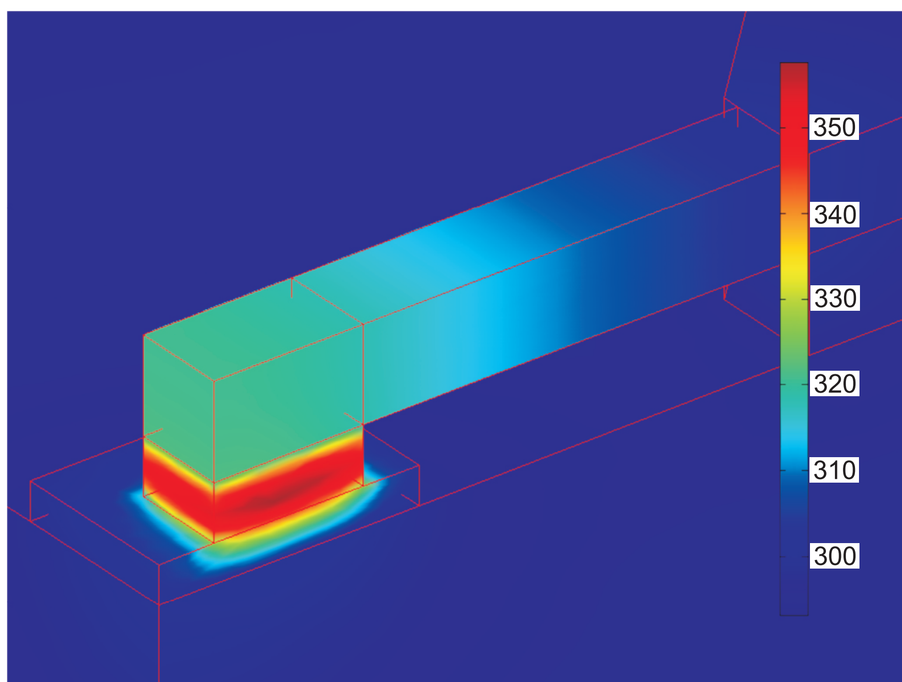

Figure 3.1: Quarter of a two-mesa HBV (symmetry) in heat transfer FEM simulations. A volume power source in the active area results in a temperature distribution where heat is centered in the active area.

3.2.1 Self-heating simulations

Two models are set up in the FEM analysis, one model for the single mesa diode and another model for the two mesa. Both setups take advantage of the device symmetry to reduce the number of calculations. The FEM heat transfer model is applied with the power distributed as a volume power source in the active areas of the diode, assuming all input power is converted to heat, see Figure 3.1. The major volumes in the models are a large brass block which serves as a heat sink, with all of the boundaries held at constant temperature $T_0 = 293.15$ K, the indium phosphide substrate, the diode active regions, i.e. the mesas in InGaAs, and the gold conductors.

For InGaAs, InP and gold the temperature dependent thermal conductivity is used.

$$\begin{aligned}\kappa_{\text{InGaAs}} &= 4.7 \cdot \left(\frac{T_0}{T}\right)^{1.375} \\ \kappa_{\text{InP}} &= 68 \cdot \left(\frac{T_0}{T}\right)^{1.48} \\ \kappa_{\text{Au}} &= 0.0586(282 - T) + 317\end{aligned}$$

The input power, mesa width and length are varied, as well as the height of the mesas, in order to represent a two or three barrier material. Then the thermal resistance, R_T is calculated from the resulting temperature rise in each

mesa $\Delta T = T_{\max} - T_0$ for each structure

$$R_{\mathrm{th}} = \frac{\Delta T}{P_{\mathrm{in}}}. \tag{3.1}$$

In order to estimate the temperature rise in the diode during RF pumping, the thermal resistance is put in to ADS harmonic balance simulations, where self-heating is implemented using Chalmers HBV electro-thermal model.

3.2.2 Electro-thermal simulations

The electrical properties of the HBV are modeled in ADS employing the quasi-empirical Chalmers HBV model combined with the electro-thermal model in harmonic balance simulations. The previously calculated thermal resistances are then put in to the electro-thermal model. In the harmonic balance simulations the diode embedding impedances are optimised for maximum conversion efficiency with regards to the diode structure. Different structures are evaluated for a fixed input power of 20 mW and pump frequency $f_p = 200$ GHz. Single mesa and two-mesa HBV diodes, with different mesa areas, and a two and three barrier material are compared with eachother, for the purpose of determining which structure will give the highest conversion efficiency without exceeding the maximum temperature increase allowed, 130 K. In Table 3.1 the material parameters used in ADS harmonic balance simulations are listed.

Table 3.1: Input parameters for HBV ADS harmonic balance model

Material property	**Value**
Modulation layer (InGaAs) relative permittivity, ε_{d}	13.9
Modulation layer thickness, l	250 nm
Modulation layer doping concentration, N_{d}	$1.4 \cdot 10^{17}$ cm^{-3}
Barrier (InAlAs) relative permittivity, ε_{b}	12.7
Barrier width, b	13 nm
Spacer layer thickness, s	5 nm
Ambient room temperature, T_0	296 K
Contact layer doping concentration, N_{c}	$1 \cdot 10^{19}$ cm^{-3}
Modulation and contact layer mobilities, μ	*According to* (2.21)

3.3 Circuit design

When the diode structure is optimised the circuit needs to be designed to achieve the optimum embedding impedances. For this purpose the circuit is divided into different circuit elements which are modeled separately and simulated in full electro-magnetic field FEM simulations in HFSS. The S-parameters from each part are then imported into ADS where they are combined with the HBV model for harmonic balance simulations. Adding one part at a time makes it possible to specify the optimum impedance values for the next part. The different circuit elements are *the realisation of the diode planar structure in a waveguide channel*, *the output probe*, *the input matching circuit*, and *the input probe.* All parts are normalised to the same port impedances in HFSS, in order to make the

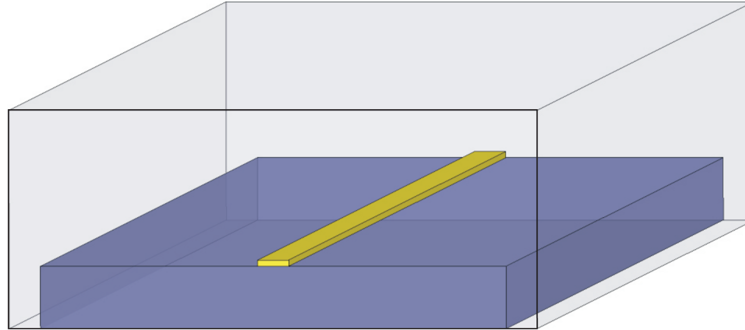

Figure 3.2: HFSS model of microstrip in waveguide structure, the outer box, i.e. the waveguide walls are modeled as perfect conducting surfaces.

specifying of the impedance at a specific point from the port straightforward, and the parts possible to combine.

In addition to the above simulations, the microstrip in the waveguide channel is simulated in HFSS, see Figure 3.3, in order to decide the channel and substrate dimensions. The waveguide dimensions are designed to serve as a high pass filter, and simulations of the propagation constant as a function of frequency provides the cut-off frequency for higher order modes. Thus the waveguide modes can be avoided and the only mode allowed to propagate through the circuit is the microstrip propagation mode.

With the intention of covering as many effects as possible in HFSS, all conductors are modeled as gold conductors, and there is an air-gap on each side of the substrate for mounting purposes. The relative permittivity of the InP substrate is defined, however the loss tangent $\tan\delta$ is not. Furthermore the walls of the waveguide are approximated to perfect conductors, see Figure 3.3.

3.3.1 Realisation of planar diode structure

The planar diode structure with two mesas and gold bridges is modeled in HFSS, see Figure 3.3, where the two diode mesas are realised as two lumped ports, normalised to 50Ω, between the conductor and the buffer layer. In order to include effects of stray capacitances in HFSS, but perform the series resistance calculations in ADS the buffer layer is approximated to a layer of gold. The other two ports are wave ports, also normalised to 50Ω, and the simulated 4-port S-matrix is later exported to ADS.

Harmonic balance simulations are performed subsequently in ADS with the 4-port S-matrix data imported from HFSS, see Figure 3.4. The simulation results include the conversion efficiency and the optimum embedding impedances for the HBV in a planar structure, at the fundamental and third harmonic.

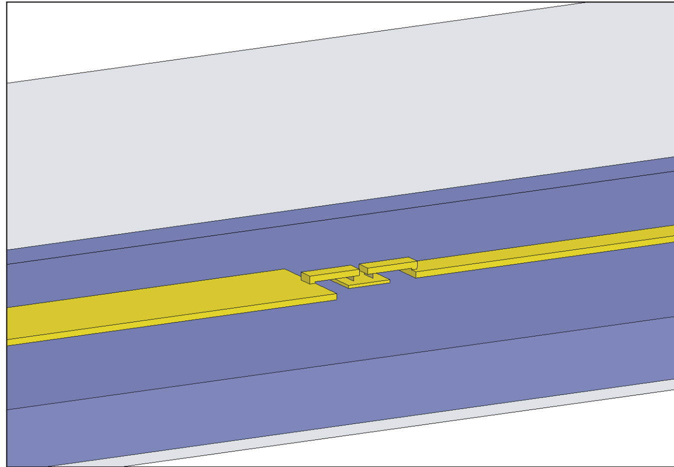

Figure 3.3: HFSS model of the planar diode with gold air-bridges, and substrate in the waveguide. The two mesas are realised as two lumped ports between the conductor and the buffer layer.

3.3.2 Input and output probe design

Both output and input probes are simulated in HFSS through several iterations of varying a parameter and just moving the reference plane at the microstrip side of the circuit. The practical parameters available are the distance from the probe to the waveguide backshort, the embedding distance at the microstrip circuit, i.e. the probe length, the conductor width and for the input probe the outer probe length and width.

The goal for the output probe is to transform the open probe end to a short circuit at the diode for the fundamental frequency, and to match the third harmonic embedding impedance, which is simulated in ADS. The finished output probe design S-parameters are then imported to the ADS harmonic balance simulation to calculate new optimum embedding impedances for the input matching circuit.

3.3.3 Input matching circuit design

For the input impedance matching circuit design an ADS model S-parameter sweep with ideal transmission line components is set up. The idea is to adapt a previous design for half the frequency, using one balanced sub and a quarter wave transformer. When the ideal circuit is optimised to fit the optimum input embedding impedances from the previous ADS simulation a second ADS simulation is set up with microstrip components and the length and widths of the microstrips are optimised to fit the result of the ideal circuit. Because the microstrip is placed in a waveguide, and because the substrate thickness is limited, there are limitations on microstrip widths and stub lengths, and the maximum and minimum widths are 130 μm and 10 μm respectively.

Next the values of the microstrip lengths and widths are put in to HFSS to perform full electro-magnetic field simulations on the circuit. If the result

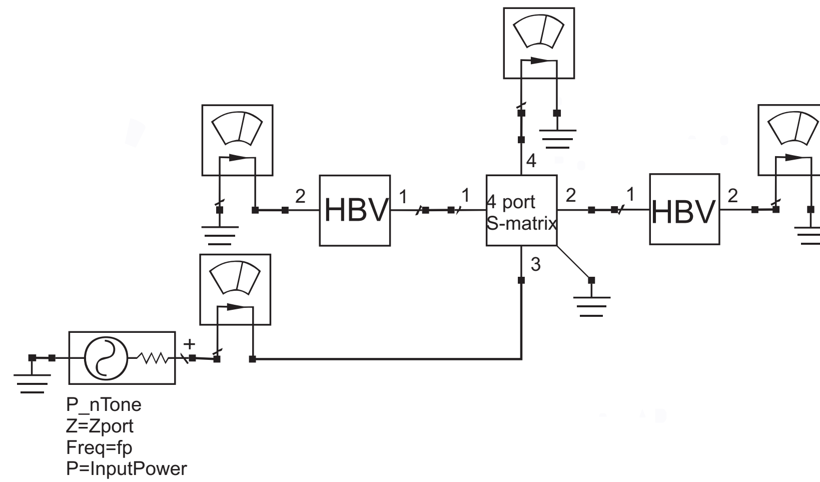

Figure 3.4: Example of ADS harmonic balance setup for optimum embedding impedances, where the 4-port S-matrix is imported from HFSS.

differs from the ADS simulation, the circuit needs to be optimised in HFSS. When the HFSS S-parameter results are close enough to the results simulated in ADS, the resulting circuit dimensions are put into ADS, and tuned again. This iterative approach gives a good idea what the change in stub lengths or microstrip widths will do for the S-parameters of the circuit, and finally result in a new input matching design.

Finally all parts, probes, diode structure and matching circuit, are put together first in ADS, then in HFSS for a full electro-magnetic field simulation, which is exported and imported to ADS for harmonic balance simulation, for the final results.

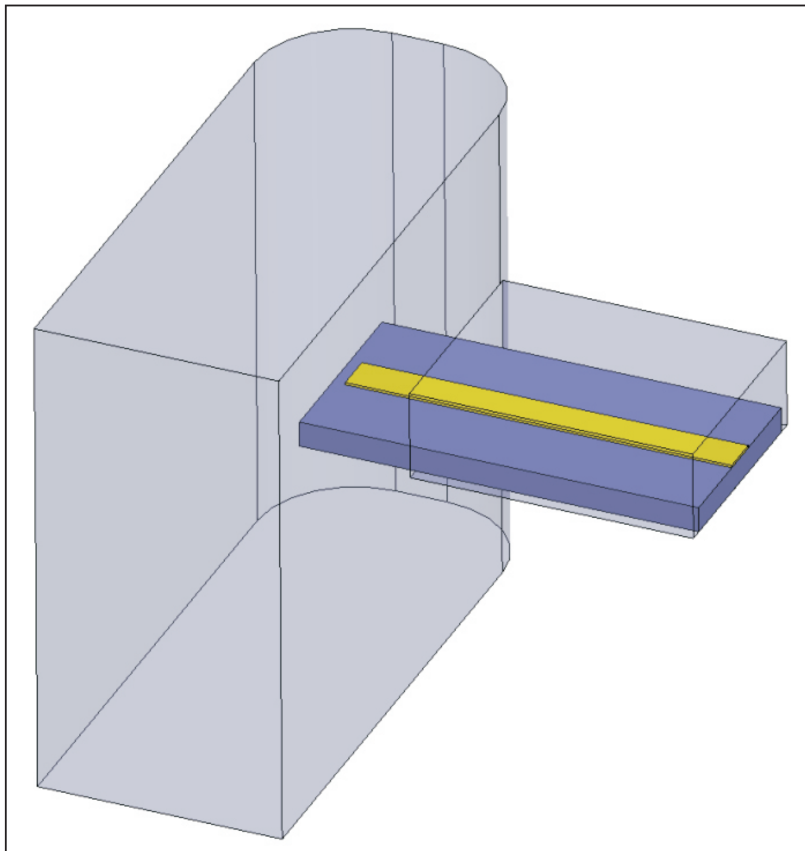

Figure 3.5: HFSS model of the output probe, and output waveguide.

Chapter 4

Results

In the following chapter the results from the material investigation, the diode design and the circuit design results are presented.

4.1 Material investigation

The preliminary material investigation resulted in a peak value for the cut-off frequency at doping concentration $N_{\mathrm{d}} = 1.7 \cdot 10^{17}$ cm^3, see Figure 4.1. This coincides with the intersection between the current saturation limited maximum depletion width at lower doping concentrations, and the impact ionisation limited depletion width at higher concentrations. Furthermore there is a fast drop in the cut-off frequency for higher doping levels, so the optimal practical value for the doping is, between $1 \cdot 10^{17}$ and $1.7 \cdot 10^{17}$ cm^3. The results also show that the impact of the modulation layer thickness on the cut-off frequency is small. Therefore the modulation layer thickness of the epi-material in Table 2.2 can be used.

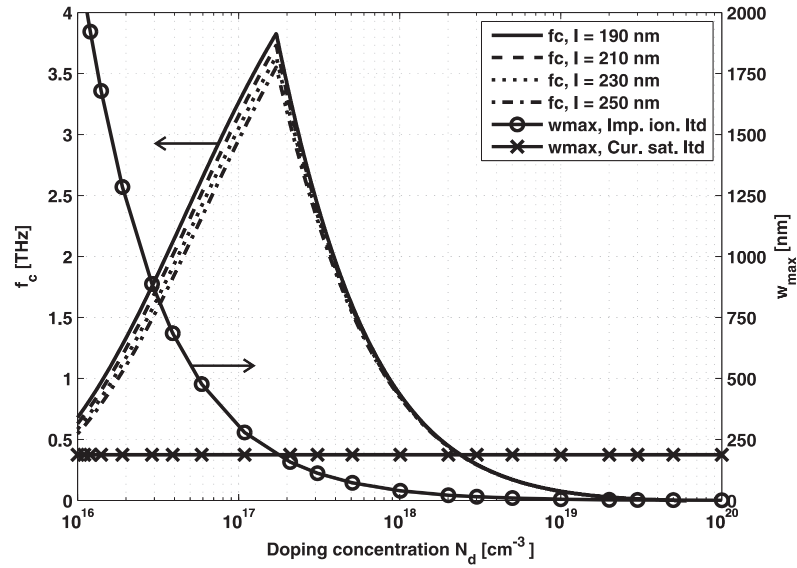

Figure 4.1: Cut-off frequency, f_c and maximum depletion width w_{max} for different doping concentrations N_d and modulation layer thickness l. HBV diode with two mesas and three barrier layers in each mesa.

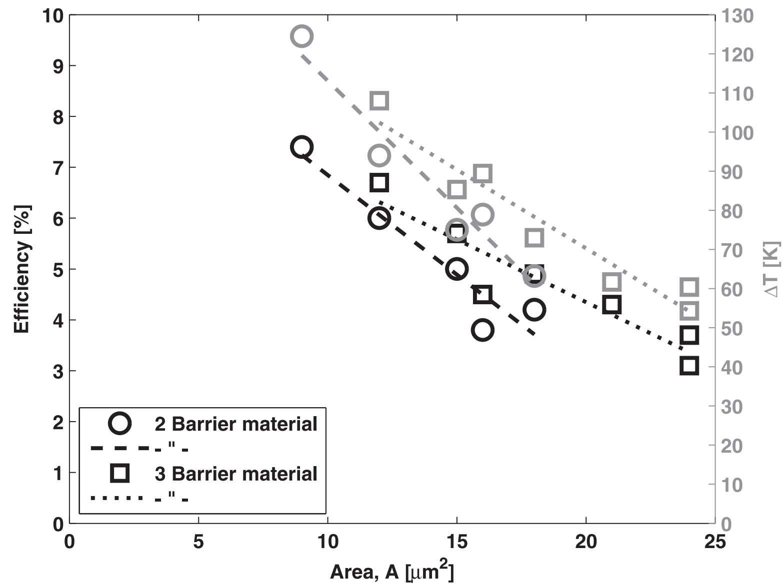

Figure 4.2: ADS harmonic balance simulation results for efficiency and self heating ΔT for different diode areas and number of barriers and a constant input power of 20 mW.

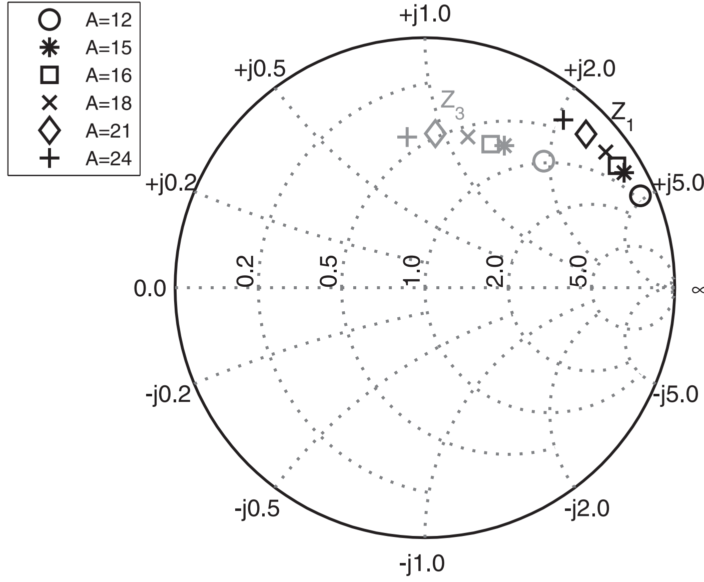

Figure 4.3: ADS harmonic balance simulation results for optimum input and output matching impedances, Z_1 and Z_3, for different diode areas.

4.2 Diode simulation results

The results of electro-thermal investigation for different HBV diode topologies in Figure 4.2 show that there is no advantage with a two-barrier material compared to the three-barrier material in Table 2.2 at 20 mW input power. Moreover, the conversion efficiency at constant input power decrease with an increase of the diode area, however the self heating and matching properties improve with larger mesa areas, see Figure 4.2 and Figure 4.3.

The efficiency increases for higher power levels, but the input power level is limited by the self heating in the diode. For one mesa diodes the advantage of a high efficiency is canceled by the large mesa area necessary to keep the self heating at a sufficiently low level. From Figure 4.2 the optimum mesa area, with regards to conversion efficiency would be about 10 μm, a larger mesa area would however be more practical from a processing and matching point of view, therefore a 5×4 μm^2 two mesa diode will be used. Moreover the well characterised three-barrier material in Table 2.2 is a good choice for this HBV diode frequency tripler.

4.3 Circuit simulation results

The results of the simulations of the different parts of the circuit are presented in figures 4.4-4.9.

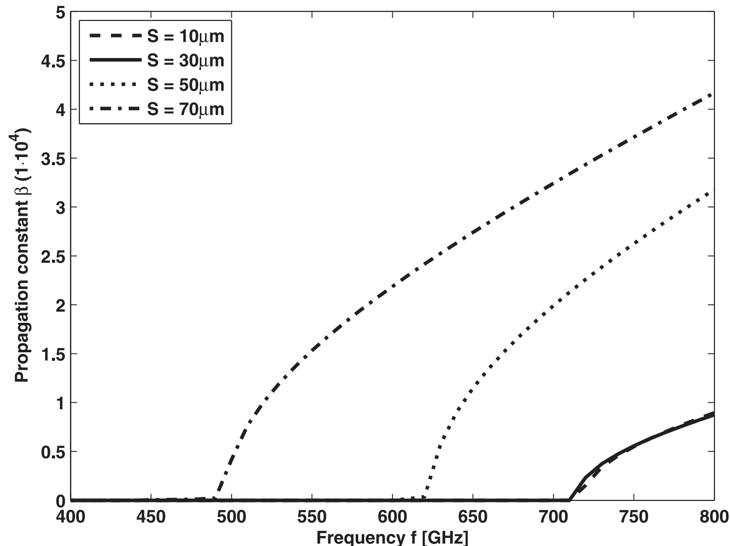

Figure 4.4: Propagation of the 2nd order mode in a microstrip with 20 μm substrate thickness in a 170×70 μm cross-section channel for different microstrip line widths.

4.3.1 Waveguide channel and substrate dimensions

The first part, waveguide channel dimensions, resulted in a waveguide channel with the cross section dimensions 170×70 μm. The waveguide channel combined with a substrate cross section of 150×20 μm and conductor width of 30 μm resulted in a higher mode cut-off frequency larger than 700 GHz, see Figure 4.4, which is enough to avoid higher order mode propagation in the channel. This implies that the maximum conductor width at the in and output waveguide can be maximum 30 μ wide in order to avoid excitation of higher modes.

4.3.2 Planar diode structure

The effect of the diode section with air-bridges and distributed mesas (simulated in HFSS) on the optimum impedances is shown in Figure 4.5. The air-bridges introduce a capacitance, which move the optimum values for the impedance match down on the Smith chart. The efficiency for the diode with air-bridges is 0.2 percent points lower than for the diode simulated without air-bridges, see Figure 4.9.

4.3.3 Input and output probes

The output probe matching is presented in Figure 4.6, where the circuit design results in a short circuit towards the output at the diode for the fundamental frequency, $Z_{1,\text{out}} \approx 0$, and a perfect match for the third harmonic, $Z_{3,\text{out}}(630\text{ GHz}) = Z_{3,\text{out}}^{\text{opt}}$. The variation over the frequency bands $200 - 220$ and $600 - 660$ GHz respectively, is small. After adding the output to the ADS

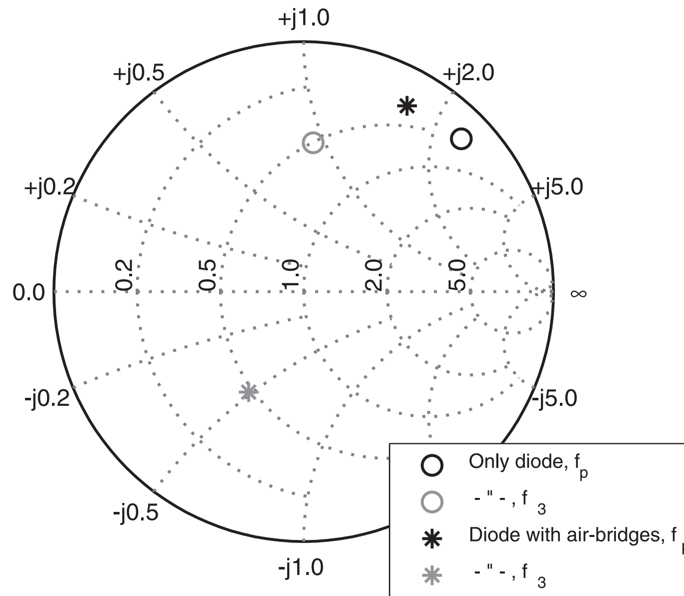

Figure 4.5: ADS combined with HFSS simulation results for the distributed diode with air-bridges compared with the pure ADS simulation of the HBV.

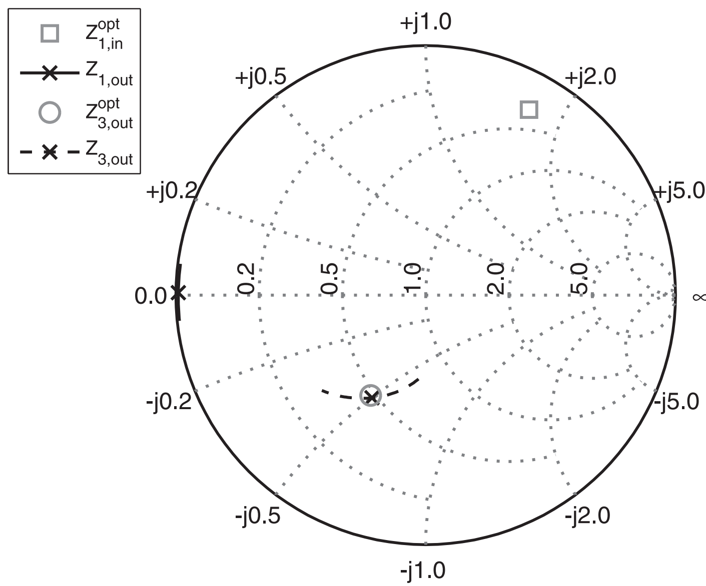

Figure 4.6: Output probe HFSS design result. The fundamental tone is a short circuit at the output, while the third harmonic is matched at the optimal impedance which was simulated in ADS. The frequency span for $Z_{1,\text{out}}$ is $200-220$ GHz, and $600-660$ GHz for $Z_{3,\text{out}}$. $\times$ marks 210 and 630 GHz respectively.

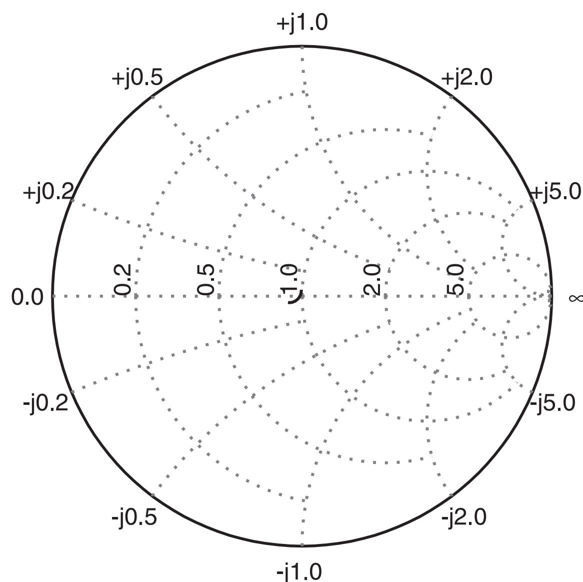

Figure 4.7: Input probe HFSS design result in the frequency span 200 − 220 GHz, normalised to 50 Ω.

harmonic balance simulation the efficiency is still the same at the center frequency, but more narrowband than before, see Figure 4.9.

The input probe converts the waveguide impedance at the input to 50 Ω on the microstrip, see Figure 4.7. The impedance change with frequency is very small, which is preferable for a broadband match with the input matching circuit.

4.3.4 Input matching circuit

The input matching circuit match the input impedance at the fundamental frequency and provides a short circuit for the third harmonic simultaneously. The short circuit match at the third harmonic is fairly broadband, $Z_{3,\mathrm{out}} \approx Z_{3,\mathrm{out}}^{\mathrm{opt}}$, and the circuit provides a slightly mismatched but broadband impedance matching, $Z_{1,\mathrm{in}}$, for the fundamental frequency at the input, see Figure 4.8. When adding the input impedance matching circuit to the design in ADS the efficiency of the HBV tripler is almost 2 %, see Figure 4.9. The efficiency drop can be explained by the mismatch at the fundamental frequency.

4.4 Final tripler circuit design results

Figure 4.10 shows the complete 3D circuit model of the HBV frequency tripler. The waveguide block will be split in the middle of the circuit parallel to the xy-plane (right across the long sides of the in and output waveguides. The much larger waveguide is the input and the smaller the output.

The result from the complete 3D model in HFSS and ADS imply that output

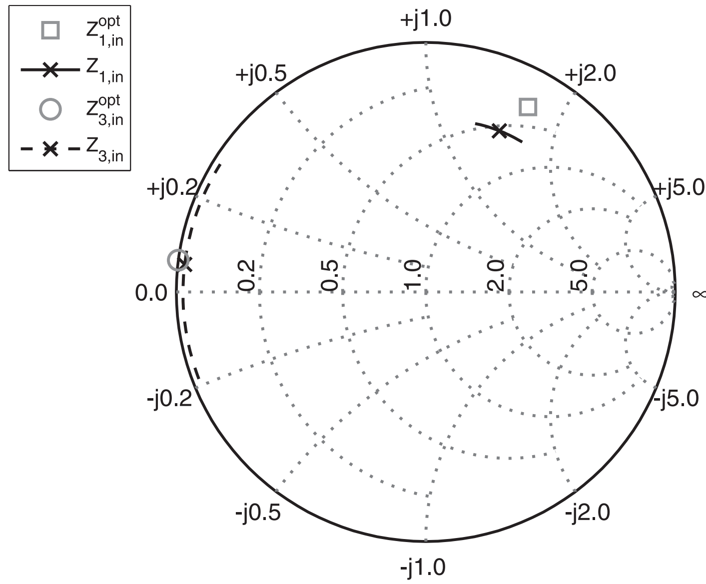

Figure 4.8: Input matching circuit HFSS design result. Both at the fundamental and the third harmonic the impedances match the optimal impedances simulated in ADS.The frequency span for $Z_{1,\mathrm{in}}$ is $200 - 220$ GHz, and $600 - 660$ GHz for $Z_{3,\mathrm{in}}$. $\times$ marks 210 and 630 GHz respectively.

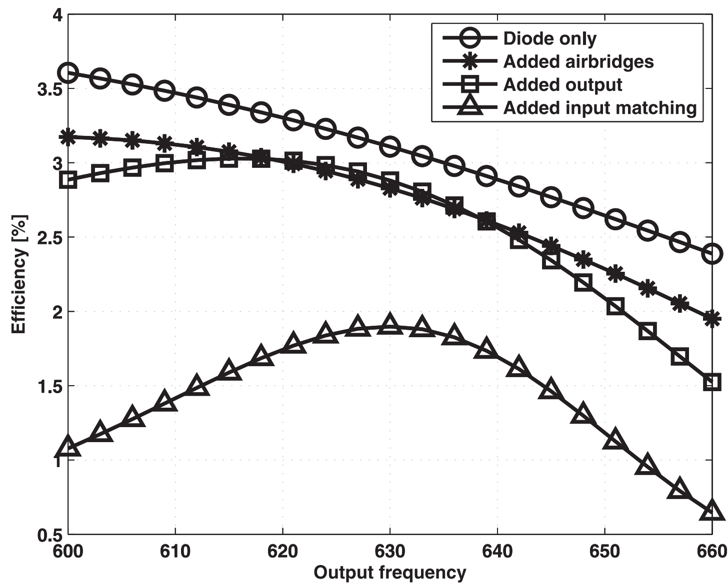

Figure 4.9: ADS harmonic balance simulation results for efficiency with the different circuit parts HFSS simulations added to the ADS harmonic balance simulation.

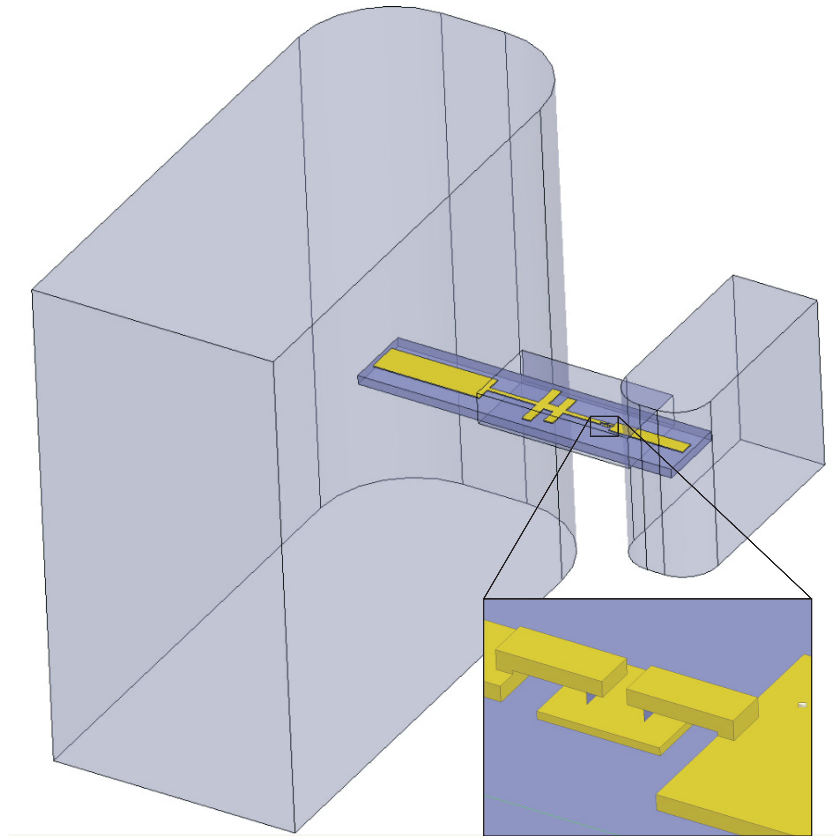

Figure 4.10: Complete circuit model in HFSS. Input waveguide is WR04 and output is WR1.5.

power and efficiency increase with the input power, and the output maximum moves up in frequency as the input power increase, see Figure 4.11. Maximum output power is 1.58 mW, and the conversion efficiency is 3 % for $P_{\text{in}} = 50$ mW.

The temperature difference for 50 mW input $\Delta T = 125$ K, see Figure 4.13. The temperature increase for higher input powers, and differ in the two different mesas due to the distributed power. However, the distributed effect may in part be a result of a limitation in the model, which does not take the thermal transfer between the two mesas into account.

Figure 4.12 shows the increase in output power at $f_3 = 630$ GHz as the input power increase, and the decrease in conversion loss with input power. The maximum return loss varies between $RL = 12$ dB for $P_{\text{in}} = 10$ mW and $RL = 9$ dB for $P_{\text{in}} = 50$ mW, see Figure 4.14.

At $P_{\text{in}} = 20$ mW the output power is -5 dBm and the conversion efficiency 1.6 %, see Figure 4.15. The half power bandwidth is 58.7 GHz or 9.5 % for a center frequency of 620 GHz.

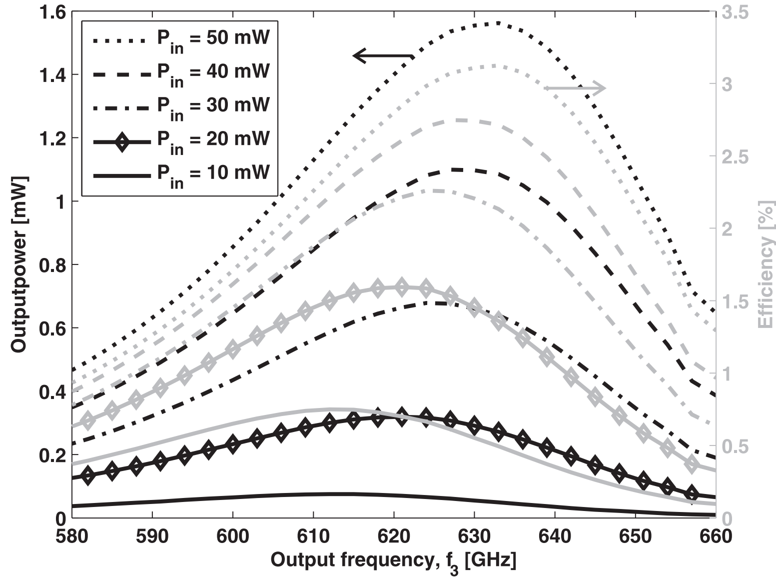

Figure 4.11: Output power and efficiency for the entire circuit for different input powers. Simulated in ADS harmonic balance simulation, combined with HFSS.

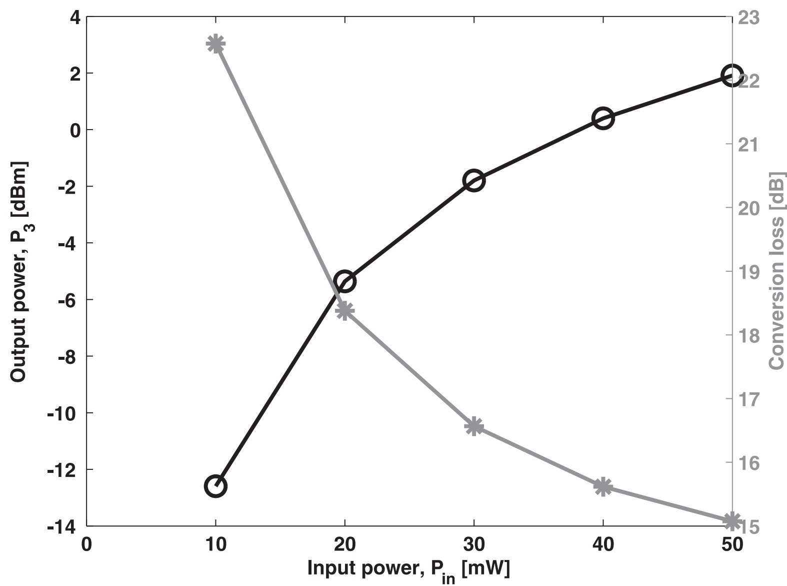

Figure 4.12: Output power and efficiency vs. input power at pumping frequency $f_3 =$ 630 GHz. Simulated in ADS harmonic balance simulation, combined with HFSS.

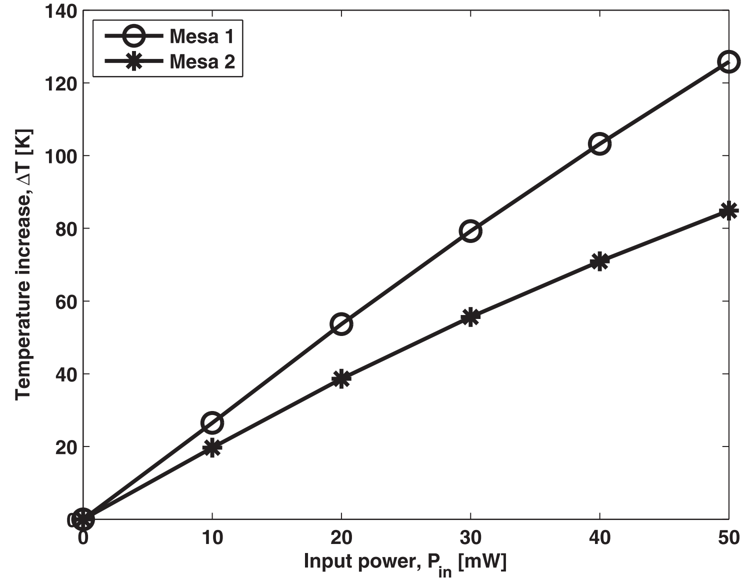

Figure 4.13: Temperature increase in each mesa for different input powers. Simulated in ADS harmonic balance simulation, combined with HFSS.

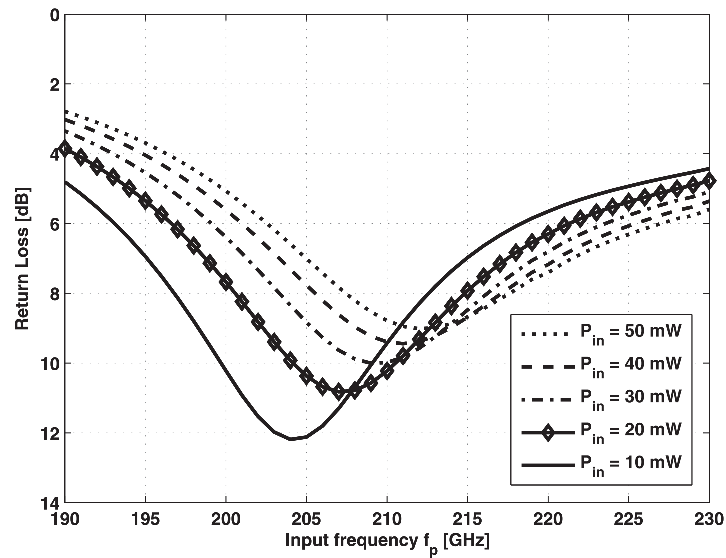

Figure 4.14: Large signal return loss at the input for the entire circuit for different input powers. Simulated in ADS harmonic balance simulation, combined with HFSS.

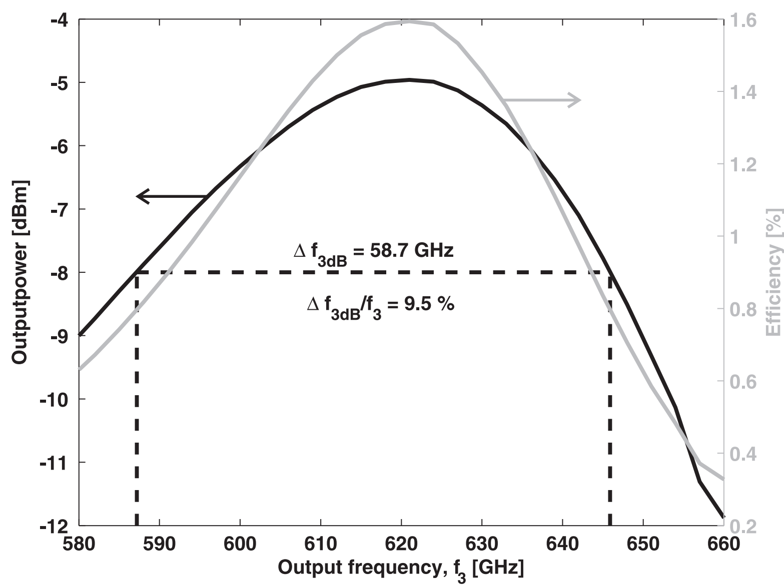

Figure 4.15: Output power and efficiency for the entire circuit with 20 mW input power. Simulated in ADS harmonic balance simulation, combined with HFSS.

Chapter 5

Discussion and conclusion

In this final chapter, the results and the method used are discussed, as well as potential improvements and the future outlook of HBV multiplier design. The chapter ends with a conclusion of the work.

5.1 Discussion

The method of combining two simulation methods when designing HBV multiplier circuits has been proven accurate in previous work, and is an indicator that the simulated results in this work are realistic. By taking advantage of the electro-magnetic field simulations in HFSS, effects caused by structural elements in the circuit can be included in the harmonic balance simulations in ADS, and provide more accurate results. The implementation of the Chalmers HBV model, combined with self heating as the non-linear device in harmonic balance simulations in ADS, have previously been used with good results for lower frequencies. However, as the frequencies increase the actual result of the effects of e.g. doping level on current saturation, heating, and of diode dimensions that are closer to the wavelength, may differ from the model. Nevertheless, the values for the designed HBV frequency tripler are reasonable, and the step by step approach illustrated in Figure 4.9 produces results that indicates that the method is valid. Also, the output power is in line with results for other varactor based multipliers, see Figure 1.1.

Assumptions made in simulations may cause the simulated results to differ from actual measured results. For instance, losses in InP was not included in the HFSS simulation, why the actual circuit may produce more losses, reducing the actual conversion efficiency. Self heating in the mesas was calculated using a worst case thermal resistance, and almost without consideration of the thermal transport between the mesas. For future improvements the resulting distributed power in the mesas can be put into another set of thermal transport FEM simulations, and an additional iteration and calculation of the thermal resistance be performed.

If the fabricated circuit proves to be lossy, one way to probably improve the design is to investigate the possibility to match input matching circuit to a lower impedance at the input probe, thereby making the line wider and less lossy. Another way to improve the design is to investigate if different size mesas

will improve the performance since, because of the distributed layout, the power applied on the separate mesas differ. Another improvement may be to taper the transmission line towards the air-bridge, and perhaps use longer air-bridges and thereby reduce the parasitic capacitance between conductors and mesas. With a reduction of parasitic capacitance, perhaps a more broadband match will be possible. However in order to investigate this, the simulation method used in this work needs some alterations.

Fabrication of this multiplier will be possible using existing processing methods for HBV MMIC. However the dimensions are much smaller than the circuits currently being fabricated in this process, which needs to be taken into consideration. For instance, one limitation may be in the alignment of air-bridge contacting on top of mesas, for which different lithography techniques may need to be investigated. Other possible issues are the difficulty in controlling the substrate thickness which for microstrip is very sensitive.

As HBV multipliers are developed for even higher frequencies in the future further development of device material and the HBV model may be necessary. The first hurdle to overcome is the waveguide mode in the substrate, and controlling the substrate thickness. Thinning down the substrate further, other circuit topologies where substrate thickness is less influential on the multiplier performance, or different materials may be the answer. Another possibility is wafer bonding, where the epitaxial active layers are transferred from the lattice matched InP substrate to substrates with lower dielectric constants, e.g. Si or quartz, before processing. An effect of this may also be better cooling of the device, if a substrate with better heat transfer properties is used.

5.2 Conclusion

A HBV frequency multiplier for an output power above 1 mW and more than 2 % conversion efficiency at 630 GHz output frequency has been designed using commercial simulation software. The resulting multiplier shows a 3 dB bandwidth of 9 %. The results are in line with previous results for HBV multipliers at lower frequencies, and with Schottky diode based multipliers at higher frequencies. Furthermore, fabrication of the multiplier may be performed with existing processing methods for HBV MMICs. For further development of HBV multipliers for higher frequencies, methods to overcome the problems of waveguide mode in the substrate, and the sensitivity for substrate thickness that exists for microstrip circuits, must be developed. In addition the self heating effects should be investigated further.

References

[1] P. H. Siegel, "Thz technology: An overview," *International Journal of High Speed Electronics and Systems*, vol. 13, no. 2, pp. 351 – 394, 2003.

[2] P. H. Siegel, "Terahertz technology," *IEEE Transactions on Microwave Theory and Techniques*, vol. 50, no. 3, pp. 910 – 928, Mar. 2002.

[3] M. Tonouchi, "Cutting-edge terahertz technology," *Nature Photonics*, vol. 1, no. 2, pp. 97 – 105, Feb. 2007.

[4] J. S. Ward, G. Chattopadhyay, J. Gill, H. Javadi, C. Lee, R. Lin, A. Maestrini, F. Maiwald, I. Mehdi, E. Schlecht, and P. Siegel, "Tunable broadband frequency-multiplied terahertz sources," in *33rd International Conference on Infrared, Millimeter and Terahertz Waves, IRMMW-THz, 2008*, Sep. 2008, pp. 1 – 3.

[5] A. Maestrini, J. Ward, J. Gill, H. Javadi, E. Schlecht, C. Tripon-Canseliet, G. Chattopadhyay, and I. Mehdi, "A 540-640-GHz high-efficiency four-anode frequency tripler," *IEEE Transactions on Microwave Theory and Techniques*, vol. 53, no. 9, pp. 2835 – 2843, Sep. 2005.

[6] E. Kollberg and A. Rydberg, "Quantum-barrier-varactor diodes for high-efficiency millimetre-wave multipliers," *Electronic Letters*, vol. 25, no. 25, pp. 1696 – 1698, 1989.

[7] J. Stake, T. Bryllert, A. i. Olsen, and J. Vukusic, "Heterostructure barrier varactor quintuplers for terahertz applications," *Proceedings of the 3rd European Microwave Integrated Circuits Conference*, pp. 206 – 209, Oct. 2008.

[8] J. Stake, T. A. Emadi, and J. Vukusic, "Terahertz generation by multiplication," in *Terahertz Frequency Detection and Identification of Materials and Objects*, R. E. Miles, X.-C. Zhang, H. Eisele, and A. Krotkus, Eds. Dordrecht, The Netherlands: Springer Netherlands, 2007, pp. 17 – 30.

[9] Virginia Diodes Inc. (2010, Apr.) Multipliers. [Online]. Available: http://www.virginiadiodes.com/

[10] J. Vukusic, T. Bryllert, T. A. Emadi, M. Sadeghi, and J. Stake, "A 0.2-W Heterostructure Barrier Varactor Frequency Tripler at 113 GHz," *IEEE Electron Device Letters*, vol. 28, no. 5, pp. 340 – 342, May 2007.

[11] M. Saglam, B. Schumann, V. Mullerwiebus, A. Megej, U. Auer, M. Rodriguez-Girones, R. Judaschke, E. J. Tegude, and H. L. Hartnagel, "450 GHz millimetre-wave signal from frequency tripler with heterostructure barrier varactors on gold substrate," *Electronics Letters*, vol. 38, no. 13, pp. 657 – 658, Jun. 2002.

[12] P. J. Penfield and R. P. Rafuse, *Varactor Applications*. Cambridge, Massachusetts: The M.I.T. Press, 1962.

[13] A. Uhlir Jr, "The potential of semiconductor diodes in high-frequency communications," *Proceedings of the IRE*, vol. 46, no. 6, pp. 1099 – 1115, Jun. 1958.

[14] J. M. Manley and H. E. Rowe, "Some general properties of nonlinear elements - part i. general energy relations," *Proceedings of the IRE*, vol. 44, no. 7, pp. 904 – 913, Jul. 1956.

[15] C. H. Page, "Harmonic Generation with Ideal Rectifiers," *Proceedings of the IRE*, vol. 46, no. 10, pp. 1738 – 1740, Oct. 1958.

[16] K. Krishnamurthi and R. G. Harrison, "Analysis of symmetric-varactor-frequency triplers," in *IEEE MTT-S International Microwave Symposium Digest, 1993.*, vol. 2, 1993, pp. 649 – 652.

[17] L. Dillner, J. Stake, and E. Kollberg, "Analysis of symmetric varactor frequency multipliers," *Microwave and optical technology letters*, vol. 15, no. 1, pp. 26 – 29, May 1997.

[18] J. Stake, S. H. Jones, L. Dillner, S. Hollung, and E. L. Kollberg, "Heterostructure-Barrier-Varactor Design," *IEEE Transactions on Microwave Theory and Techniques*, vol. 48, no. 4, pp. 677 – 682, Apr. 2000.

[19] S. M. Sze and K. K. Ng, *Physics of semiconductor devices*, 3rd ed. Hoboken, New Jersey: John Wiley & Sons, Inc., 2007.

[20] Y. Fu, J. Stake, L. Dillner, M. Willander, and E. L. Kollberg, "AlGaAs/GaAs and InAlAs/InGaAs Heterostructure Barrier Varactors," *Journal of Applied Physics*, vol. 82, no. 11, pp. 5568 – 5572, Dec. 1997.

[21] T. A. Emadi, T. Bryllert, M. Sadeghi, J. Vukusic, and J. Stake, "Optimum barrier thickness study for the InGaAs/InAlAs/AlAs heterostructure barrier varactor diodes," *Applied Physics Letters*, vol. 90, no. 1, Jan. 2007.

[22] M. Sotoodeh, A. H. Khalid, and A. A. Rezazadeh, "Empirical low-field mobility model for III-V compounds applicable in device simulation codes," *Journal of Applied Physics*, vol. 87, no. 6, pp. 2890 – 2900, Mar. 2000.

[23] M. Ingvarson, J. Vukusic, A. Olsen, T. Emadi, and J. Stake, "An electrothermal HBV model," in *2005 IEEE MTT-S International Microwave Symposium, Vols 1-4*, 2005, pp. 1151 – 1153.

[24] J. Stake, L. Dillner, S. Jones, C. Mann, J. Thornton, J. Jones, W. Bishop, and E. Kollberg, "Effects of self-heating on planar heterostructure barrier varactor diodes," *IEEE Electron Device Letters*, vol. 45, no. 11, pp. 2298 – 2303, Nov. 1998.

[25] E. F. Schubert. (2010, Dec.) Light emitting diodes. [Online]. Available: http://www.lightemittingdiodes.org/

[26] J. Liljedahl, T. Bryllert, J. Vukusic, and J. Stake, "Development of a HBV tripler for 0.6 THz," in *21st International Symposium on Space Terahertz Technology, Oxford, UK*, Mar. 2010, pp. 454 – 459.

[27] (2011, Mar.) Electronic archive. New semiconductor materials. Characteristics and properties. Ioffe Physico-Technical Institute. [Online]. Available: http://www.ioffe.rssi.ru/SVA/NSM/

[28] Y. Fu, M. Mamor, M. Willander, S. Bengtsson, and L. Dillner, "n-Si/SiO2/Si heterostructure barrier varactor diode design," *Applied Physics Letters*, vol. 77, no. 1, pp. 103 – 105, Jul. 2000.

[29] M. Mamor, Y. Fu, O. Nur, M. Willander, and S. Bengtsson, "Leakage current and capacitance characteristics of Si/SiO2/Si single-barrier varactor," *Applied Physics A: Materials Science & Processing*, vol. 72, pp. 633 – 637, 2001.

[30] J. G. Champlain, R. Magno, M. Ancona, H. S. Newman, and J. B. Boos, "InAs-based heterostructure barrier varactor diodes with In0.3Al0.7As0.4Sb0.6 as the barrier material," *Solid-state Electronics*, vol. 52, no. 11, pp. 1829 – 1832, Nov. 2008.

[31] M. Dastjerdi, A. Sanz-Velasco, J. Vukusic, E. Kollberg, M. Sadeghi, and J. Stake, "InGaAs/InAlAs/AlAs Heterostructure Barrier Varactors on Silicon Substrate," *IEEE Electron Device Letters*, vol. 32, no. 2, pp. 140 –142, 2011.

[32] R. E. Collin, *Foundations for microwave engineering*, 2nd ed. Hoboken, New Jersey: John Wiley & Sons, Inc., 2001.

[33] R. Pucel, "Design Considerations for Monolithic Microwave Circuits," *IEEE Transactions on Microwave Theory and Techniques*, vol. 29, no. 6, pp. 513 – 534, Jun. 1981.

[34] V. Balynas, A. Krotkus, A. Stalnionis, A. T. Gorelionok, N. M. Shmidt, and J. A. Tellefsen, "Time-resolved, hot-electron conductivity measurement using an electro-optic sampling technique," *Applied Physics A: Materials Science & Processing*, vol. 51, pp. 357 – 360, 1990.

Appendix A

Paper A

Development of a HBV tripler for 0.6 THz

J. Liljedahl, T. Bryllert, J. Vukusic and J. Stake

in *21st International Symposium on Space Terahertz Technology, ISSTT 2010, Oxford, UK*, pp. 454-459, March, 2010.

Development of a HBV tripler for 0.6 THz

Johanna Liljedahl*, Tomas Bryllert, Josip Vukusic and Jan Stake
Dept. of Microtechnology and Nanoscience, Chalmers University of Technology, Göteborg, Sweden
*Contact: johanna.liljedahl@chalmers.se, phone +46(0)31 772 18 75

***Abstract*—We report on the progress of the design of a HBV frequency tripler for 0.6 THz. The diode is based on the InGaAs/InAlAs/AlAs on InP material system, and the diode material and geometry has been optimised with regards to conversion efficiency. In designing the diode, it was found that self heating is the major limiting factor due to the poor thermal conductivity of InGaAs. The resulting HBV is a two-mesa diode from a three-barrier material, with a mesa area of 6×3 μm^2, and is estimated to have a 6-7% conversion efficiency and 100 - 150 K self heating at an input power of 30 mW.**

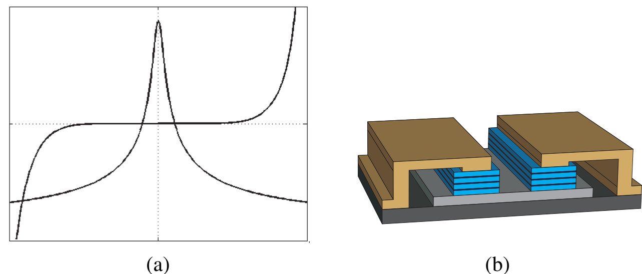

(a) (b)

Fig. 1. (a) C-V and I-V curve for a HBV diode. C-V is symmetric while I-V is antisymmetric. (b) Model of a two-mesa HBV diode with a total of six barriers, and gold air bridges. (The model is not according to scale)

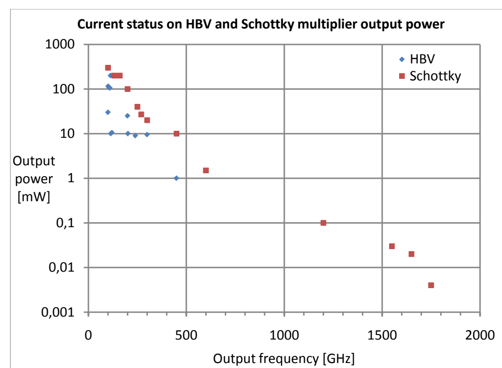

Fig. 2. Current status on output power for single diode HBV frequency multipliers and Schottky diode frequency multiplier chains [7][8][9][5].

I. Introduction

The trend in recent space observing projects is to cover frequencies in the terahertz (THz) gap. In many observing applications the high spectral resolution from heterodyne receivers is desired. However, when going from millimetre to sub-millimetre wavelengths there is a lack of fundamental LO sources above 200 GHz. Therefore the most commonly used and efficient solution for LO signal sources is frequency upconversion through multiplication by non-linear semiconductor devices [1].

Today most frequency multiplier circuits are realized using Schottky diodes. Due to their high performance, balanced Schottky doublers have become standard as multiplier sources, and planar Schottky diode multipliers for the THz frequency range have been demonstrated [2].

An alternative to the Schottky diode is the Heterostructure Barrier Varactor (HBV). Ever since the invention in 1989, the HBV diode has been promising for frequency multiplication to THz frequencies [3]. Today HBV diodes are used as high power multipliers for frequencies up to and above 200 GHz [4].

The HBV consists of a wide bandgap semiconductor barrier spaced between two narrow bandgap, equally doped, semiconductor modulation layers. The C-V curve is symmetric, while the I-V curve is anti-symmetric, and these properties cause the HBV to only generate odd harmonics. Thereby, when used as a frequency tripler, there is only need for circuit matching at the in and output frequencies, and no idler matching is needed. In addition, there is no need for DC-biasing, which together with the matching requirements enables a simple and compact circuit design, making it ideal for space applications.

Another advantage is that the sandwich structure of the HBV allows stacking of several diodes for better power handling capability, and at the same time diode miniaturisation is prevented [5]. Nevertheless, the highest output frequency published for HBV diode based multipliers is 450 GHz [6]. Our aim is to push this limit further into the sub-mm region.

We present the current status on the development of an HBV tripler for an output frequency of 600-700 GHz. The designed HBV is based on the InGaAs/InAlAs/AlAs epitaxially grown on InP material system. The doping and layer structure impact on the conversion efficiency has been evaluated, and consideration of the effects of self heating has been crucial when choosing an appropriate diode design. The HBV diode is implemented in a MMIC circuit containing matching and filtering elements.

II. 0.6 THz HBV tripler development

In developing a 600 GHz frequency tripler there are several constraints to consider. At this high input frequency, 200-220 GHz, the available power is estimated to be less than 40 mW, which together with impedance boundaries limits the size and geometry of the diode. The high frequency makes it unsuitable for the otherwise commonly used flip chip soldering, hence the HBV frequency tripler is implemented using a monolithic

approach which offers high repeatability.

For the circuit design we decided to use conventional technology, with the advantage of having good heat sinking properties and already established designs to fall back on. The tripler will consist of a waveguide block, with waveguide in and outputs, and the matching circuit and HBV on a microstrip MMIC in a waveguide channel, coupled into the waveguides by probes.

We have limited ourselves to the use of the InGaAs/InAlAs/AlAs epitaxially grown on an InP substrate material system. The advantages of this material are the high mobility of InGaAs and the height of the energy bandgap barrier.

An effort to analytically optimise the material structure with regards to the conversion efficiency for an input frequency of 200 GHz has been made. This optimised material, material A was then compared to an already grown material, material B, to evaluate the necessity of growing a new material. The existing Material B has been verified in I-V and C-V measurements.

In comparing the two materials the effects of self heating were taken into account through FEM heat transfer modelling combined with harmonic balance simulations in ADS. In these simulations the diode geometry was investigated as well.

Finally the optimum embedding impedances for the HBV diode tripler configuration has been determined to maximise the conversion efficiency. For these simulations a 3-D model of the diodes including air bridges have been modelled in Ansoft HFSS for S-parameter extraction, combined with harmonic balance simulations in ADS.

III. Material verification

The material in Table I, earlier introduced as Material B, has been verified in I-V and C-V measurements, see figure 3. For these measurements single mesa test diodes were fabricated with different areas and measured in a probe station with an I-V and a LCR meter. The maximum capacitance of the HBV material was measured to be $C_{max} = 0.9$ fF/μm^2, and the breakdown voltage $V_{br} = \pm 19$ V (for 3 barriers). From the C-V measurements the doping concentration was extracted, $N_d = 1.4 \cdot 10^{17}$ cm^{-3}, which is slightly higher than the specification. The extracted value for the doping was then used when evaluating the material in harmonic balance simulations, described below.

IV. Diode optimisation

The HBV tripler will be pumped with at a frequency of 200-220 GHz, and at this frequency the expected available input power is about 20-40 mW. Thus the diode is optimised for an input power of 30 mW. Diode parameters such as the epi-layer structure, size and geometry have been examined in order to ensure large conversion efficiency. Furthermore, the advantage of growing a new frequency optimised material, versus using a material that has already been fabricated, but is optimised for a lower frequency range, has been evaluated.

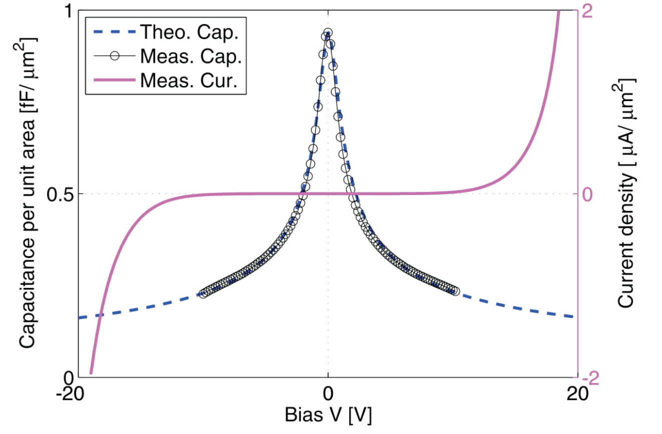

Fig. 3. I-V and C-V measurement result plus the theoretical C-V curve using the extracted doping.

A. Epi-layers

1) Barrier: The barrier material in the epi-layer design consists of a 3 nm thin layer of AlAs in the middle of two layers of 50 nm $In_{0.52}Al_{0.48}As$. The AlAs prevents leakage current by increasing the energy bandgap, but this barrier layer is lattice mismatched to InAlAs, so in order to keep it strained the thickness is limited. This optimum barrier design for the InGaAs/InAlAs/AlAs HBV material system is further described in [10] and [11], and has not been treated within this work.

2) Modulation layers: A figure of merit for a varactor diode design is the dynamic cut-off frequency [12]

$$f_c = \frac{S_{max} - S_{min}}{2\pi R_S}. \tag{1}$$

It is derived from the equivalent circuit of a varactor with a variable reactance, $C(v) = \frac{1}{S(v)}$, connected in series with a resistance, R_S.

The cutoff frequency dependence of the conversion efficiency can be estimated by

$$\eta \approx \frac{100}{1 + \alpha \left(\frac{f_p}{f_c}\right)^{\beta}} \% \tag{2}$$

where f_p is the pumping frequency, f_c the cutoff frequency, $\alpha = 200$ and $\beta = 1.5$ [13]. So in order to achieve a high efficiency, the cutoff frequency should be maximised, which is done by maximising the difference in elastance and minimising the series resistance.

The series resistance consists of several resistance elements

$$R_S = R_{active} + R_{spread,buff} + R_{contact} \tag{3}$$

where the resistance in the epi-layers is

$$R_{active} = \sum_n \frac{l_n}{\mu_n N_n q A} \tag{4}$$

n is the layer number, l_n the layer thickness, μ_n the layer mobility, N_n the layer doping and A the mesa area. The

spreading resistance between two mesas or mesa and contact for a single mesa diode is

$$R_{spread,buff} = \frac{l_{buff}}{\mu_{buff} N_{buff} q A_{buff}} \quad (5)$$

and the ohmic contact resistance is

$$R_{contact} = N_m \frac{r_c}{A} \quad (6)$$

where N_m is the number of mesas and $r_c = 100\ \Omega\text{-}\mu\text{m}^2$. The mobility is doping dependent and estimated according to [14].

The minimum elastance is determined by the Debye length, L_D,

$$S_{min} = \frac{N}{A}\left(\frac{b}{\varepsilon_b} + \frac{2s}{\varepsilon_d} + \frac{2L_D}{\varepsilon_d}\right) \quad (7)$$

while the maximum elastance is determined by the maximum depletion width, w_{max}, [13]

$$S_{max} = \frac{N}{A}\left(\frac{b}{\varepsilon_b} + \frac{2s}{\varepsilon_d} + \frac{w_{max}}{\varepsilon_d}\right). \quad (8)$$

N is the number of barriers, A the diode area, b and s the barrier and spacer thickness respectively, and ε the dielectric constants for the different materials. The maximum depletion width is limited by impact ionization, which is doping dependent, and by the current saturation which can be approximated to be constant with regards to the doping level for a constant pumping frequency [13]. This means that for doping levels above a certain value the cutoff frequency is impact ionization limited and below that frequency it is limited by the current saturation. These two criterions can be combined to estimate the optimum doping level for a high cutoff frequency, see figure 4.

This model indicates that the difference in modulation layer thickness has little impact on the conversion efficiency compared to for example the number of barriers, i.e. HBV diodes stacked in series. In order to minimise the series resistance, an optimised modulation layer thickness has the same value as the maximum depletion width, and the cut-off frequency decreases for thicker layers. While the cut-off frequency increases with the number of barriers. However, as the number of barriers increase, so does the input power necessary to drive the HBV. Therefore we chose to compare conversion efficiency for HBV diodes with different geometries, made of a two-barrier material with a modulation layer thickness of 190 nm and doping of $1.4 \cdot 10^{17}$ cm^{-3}, i.e. Material A, and the three-barrier material we already have, Material B (see Table I).

B. Device geometry

In deciding the geometry of the HBV diode taking the effects of self heating into account is crucial due to the poor thermal conductivity of InGaAs. Using heat transfer FEM simulations combined with ADS harmonic balance simulations the heating in the diode active region and the conversion efficiency has been estimated, and an appropriate geometry found.

TABLE I
HBV ACTIVE LAYER MATERIAL SPECIFICATION, MATERIAL B

Layer	Material	Thickness [Å]	Doping [cm^{-3}]	Comment
1	$In_{0.53}Ga_{0.47}As$	2,500	10^{17}	Modulation
2	$In_{0.53}Ga_{0.47}As$	50	Undoped	Spacer
3	$In_{0.52}Al_{0.48}As$	50	Undoped	Barrier
4	AlAs	30	Undoped	Barrier
5	$In_{0.52}Al_{0.48}As$	50	Undoped	Barrier
6	$In_{0.53}Ga_{0.47}As$	50	Undoped	Spacer
7-18	... 2 × Layers 1 - 6 ...			
19	$In_{0.53}Ga_{0.47}As$	2,500	10^{17}	Modulation

1) Self heating: In the FEM heat transfer model the power distributed as a volume power source, assuming all input power is converted to heat, see Figure 5. The resulting temperature is then used to calculate the thermal resistance, R_T of the diode, and the thermal resistance is then put in to ADS harmonic balance simulations where self heating is implemented using Chalmers HBV electro-thermal model to calculate the rise in temperature under RF pumping [15]. In the heat transfer simulations the temperature dependent thermal conductivity is used for InGaAs, InP and gold.

$$\begin{aligned} \kappa_{InGaAs} &= 4.7 \cdot \left(\frac{T_0}{T}\right)^{1.375} \\ \kappa_{InP} &= 68 \cdot \left(\frac{T_0}{T}\right)^{1.48} \\ \kappa_{Au} &= 0.0586(282 - T) + 317 \end{aligned}$$

2) Harmonic balance: The electrical properties of the HBV are modeled in ADS with the quasi-empirical Chalmers HBV model [16]

$$V(Q) = N\Big\{\frac{bQ}{\varepsilon_b A} + 2\frac{sQ}{\varepsilon_d A} + Sign(Q) \cdot \Big(\frac{Q^2}{2qN_d\varepsilon_d A^2} + \frac{4k_BT}{q}\Big(1 - \exp\Big[-\frac{|Q|}{2L_D A q N_d}\Big]\Big)\Big)\Big\} \quad (9)$$

These simulations also provides a value for the optimum embedding impedances for a maximised conversion efficiency.

Different geometries have been evaluated for a fixed input power of 40 mW and pump frequency $f_p = 200$ GHz. We have examined one and two-mesa HBV diodes, with different mesa areas, of Material A and B, to determine which geometry will give the highest conversion efficiency without exceeding the maximum temperature increase allowed, $130 - 150$ K. For each geometry the efficiency improves when the area decreases, see Figure 6. However only the geometry and areas where the temperature limit has not been reached are interesting, consequently the one-mesa geometry could be ruled out immediately since the area required results in a very low conversion efficiency of the HBV diode.

The best conversion efficiency geometry was chosen, a two-mesa HBV with a mesa area of $6 \times 3\ \mu$m^2, where the larger dimension sets the width of the air bridges. As can be seen in figure 6, the difference in efficiency is not very large, why we choose to use the epi-material we already have, Material B, rather than fabricate a new material.

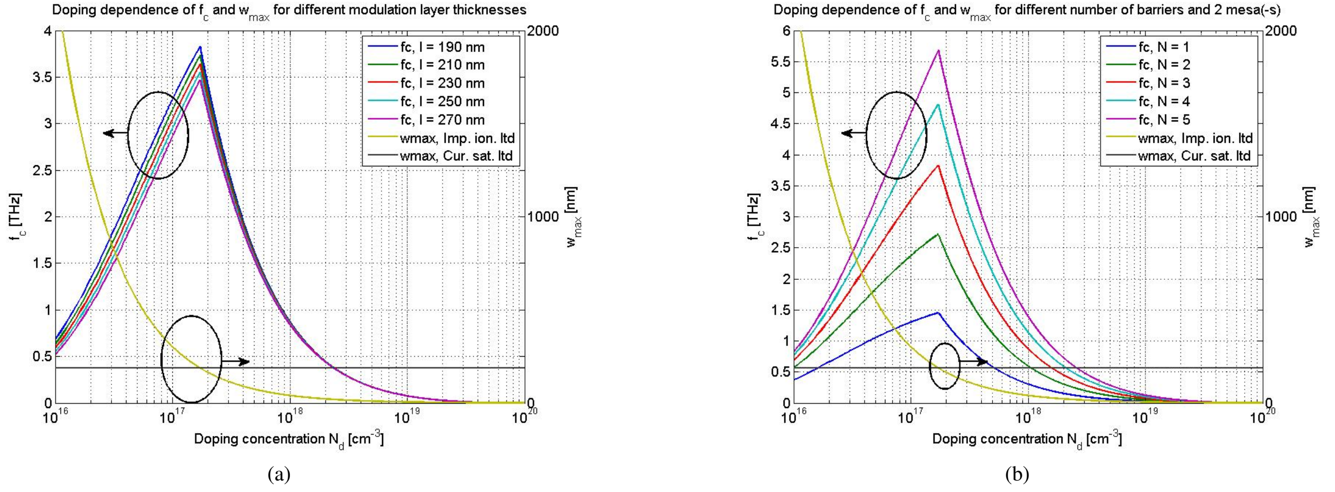

Fig. 4. Cutoff frequency and maximum depletion layer width dependence on modulation layer doping level. To the left of the intersection the cutoff frequency is current saturation limited, and to the right the cutoff frequency is impact ionization limited. $f_p = 200$ GHz, $A = 18\ \mu\text{m}^2$. (a) Cutoff frequency for different thickness of the modulation layers. $N = 3$, $N_m = 2$. (b) Cutoff frequency for different number of barriers per mesa. $l = 190$ nm, $N_m = 2$.

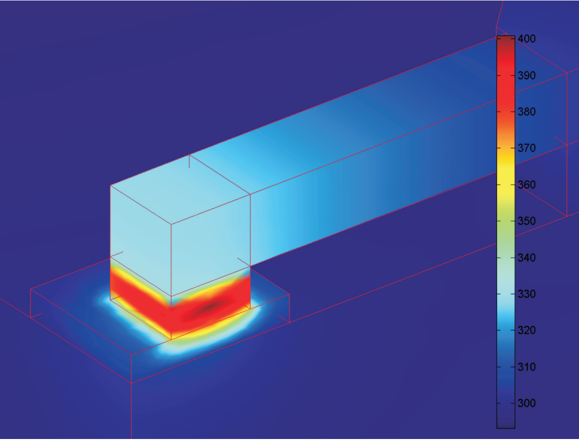

Fig. 5. Heat transfer FEM simulation of a two-mesa HBV diode. Clearly shows how the heat is concentrated in the active layers of the HBV. The image shows quarter of a diode, due to symmetry.

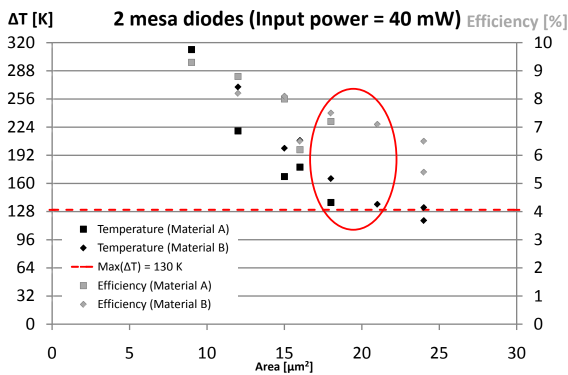

Fig. 6. Efficiency and temperature comparison of two-mesa diodes with different mesa areas and two different materials: A two-barrier material optimised for an input frequency of 200 GHz, and the 3-barrier material described in Table I. It shows that the area needs to be at least 18 μm^2 to not overheat, and that the 3-barrier material we already have can be used.

V. Circuit

While HBV diodes for lower frequencies often are separately flip chip soldered to a circuit of another material, e.g. quartz, integration of the HBV diode on a MMIC is preferable for THz frequencies. As the frequency gets higher soldering uncertainty and losses are eliminated. This means that we are limited to a InP substrate which has a large dielectric constant, so in order to reach reasonable line widths and impedances, and to avoid waveguide modes in the substrate, the substrate needs to be thin.

We will design a classic waveguide-to-microstrip-to-waveguide circuit, with all matching elements fabricated on the microstrip MMIC. The waveguide dimensions are WR-4 at the input and WR-1.5 at the output. The channel width and height is 160 μm. The design is similar to the design in [17].

A. Substrate

The most common way to thin down a substrate is either mechanically, through lapping of the back of the substrate, or through membrane technology where the back side of the substrate is etched away until a stop layer is reached deciding the substrate thickness. As InP is a brittle material there is some concern when thinning it down too thin. And as for membrane technology there are also some issues regarding the background doping of the eptiaxially grown InP layer. We do not have access to Fe-doped InP epi-material, which means the membrane will be lossy.

We have decided to move forward with a 20 μm thick substrate, which we can lap down mechanically with good precision. Propagation constant simulations in Ansoft HFSS show that 20 μm is small enough to avoid waveguide modes in the substrate for strip widths smaller than about 40 μm in a waveguide 160 μm wide, but still large enough to have a reasonable tolerance.

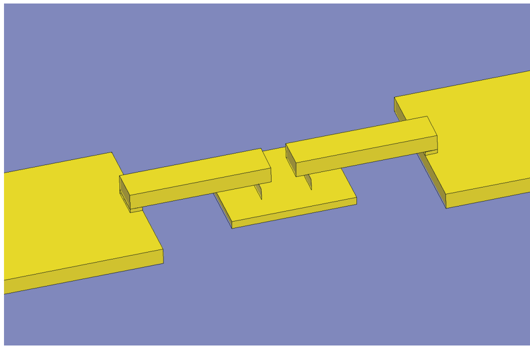

Fig. 7. HBV diode HFSS model with airbridges for deembedding optimum impedances.

B. Diode embedding impedance

The optimum HBV diode embedding impedance has been estimated in order to achieve maximum conversion efficiency at an input power of 30 mW in order keep good efficiency over the whole $20-40$ mW region. The input and output matching impedance for the fundamental tone at 200 GHz and third harmonic has been calculated in S-parameter simulations in Ansoft HFSS combined with harmonic balance simulations in ADS of the chosen geometry, a two-mesa diode of the three-barrier material (Material B). The air bridges are included in the S-parameter simulation, see Figure 7, in order to have them included in future matching circuit simulations. The HBV diode mesas are replaced with lumped ports in this simulation, and the HBV model in (9) is used in ADS. The length of the air bridges is 12 μm, the width is 4 μm, the mesa area is 6×3 μm^2, the distance between the mesas is 3 μm, pump frequency f_p = 200 GHz and the input power is 30 mW. The thermal resistance put in to the device is a "worst case" thermal resistance calculated from an input power of 40 mW on the same diode area, $R_T = 4474$ K/W.

The resulting optimum impedances at the fundamental and third harmonic, for an input frequency of 200 GHz is displayed in Figure 8.The conversion efficiency at these impedances is $\eta > 6\%$ and the self heating in the HBV diode is $100 < \Delta\ T < 150$ K.

VI. Conclusion

A HBV frequency tripler with an output frequency of 0.6 THz is currently under development. Investigations of material and diode layout show that self heating is a major limiting factor for reaching high conversion efficiency and power levels at higher frequencies. The 3-barrier epi-material developed for operation at lower frequencies can be used for the HBV and provide a theoretical conversion efficiency of 6-7% for a 2-mesa HBV diode. At an expected input power of 30 mW this will result in a outputpower of about 1 mW.

The circuit developed for the tripler is a waveguide-to-microstrip MMIC-to-waveguide circuit. The matching circuitry on the MMIC is under development and when that is done the HBV tripler will be fabricated at MC2, Chalmers.

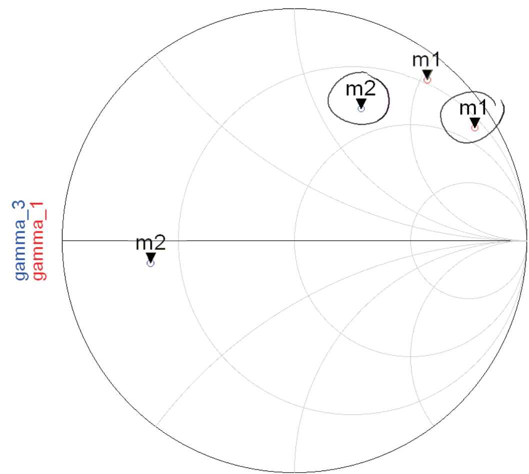

Fig. 8. HBV optimum embedding impedances for maximised efficiency at 30 mW input power and f_p = 200 GHz. m1 marks the input matching impedance for fundamental tone, and m2 the output impedance at the third harmonic including and excluding (circled) air bridges.

Acknowledgment

The authors would like to thank the Swedish Research Council (VR) and MSB "ISSI" for funding this research.

References

[1] P. H. Siegel, "THz Technology: An Overview," *International Journal of High Speed Electronics and Systems*, vol. 13, no. 2, pp. 351–394, 2003.

[2] A. Maestrini, J. Ward, J. Gill, H. Javadi, E. Schlecht, C. Tripon-Canseliet, G. Chattopadhyay, and I. Mehdi, "A 540-640-ghz high-efficiency four-anode frequency tripler," *Microwave Theory and Techniques, IEEE Transactions on*, vol. 53, no. 9, pp. 2835 – 2843, sept. 2005.

[3] E. Kollberg and A. Rydberg, "Quantum-Barrier-Varactor Diodes for High-Efficiency Millimetre-Wave Multipliers," *Electronic Letters*, vol. 25, no. 25, pp. 1696–1698, 1989.

[4] J. Stake, T. Bryllert, A. i. Olsen, and J. Vukusic, "Heterostructure barrier varactor quintuplers for terahertz applications," *Proceedings of the 3rd European Microwave Integrated Circuits Conference*, pp. 206 – 209, oct. 2008.

[5] J. Vukusic, T. Bryllert, T. A. Emadi, M. Sadeghi, and J. Stake, "A 0.2-W heterostructure barrier varactor frequency tripler at 113 GHz," *IEEE ELECTRON DEVICE LETTERS*, vol. 28, no. 5, pp. 340–342, MAY 2007.

[6] M. Saglam, B. Schumann, V. Mullerwiebus, A. Megej, U. Auer, M. Rodriguez-Girones, R. Judaschke, E. Tegude, and H. Hartnagel, "450 ghz millimetre-wave signal from frequency tripler with heterostructure barrier varactors on gold substrate," *Electronics Letters*, vol. 38, no. 13, pp. 657 –658, Jun 2002.

[7] J. S. Ward, G. Chattopadhyay, J. Gill, H. Javadi, C. Lee, R. Lin, A. Maestrini, F. Maiwald, I. Mehdi, E. Schlecht, and P. Siegel, "Tunable broadband frequency-multiplied terahertz sources," *Infrared, Millimeter and Terahertz Waves, 2008. IRMMW-THz 2008. 33rd International Conference on*, pp. 1 – 3, sept. 2008.

[8] J. Stake, T. A. Emadi, and J. Vukusic, "Terahertz generation by multiplication," in *Terahertz Frequency Detection and Identification of Materials and Objects*, R. E. Miles, X.-C. Zhang, H. Eisele, and A. Krotkus, Eds. Dordrecht, The Netherlands: Springer Netherlands, 2007, pp. 17–30.

[9] V. D. Inc., "Multipliers," available: http://www.virginiadiodes.com/, Date: April 13 2010.

[10] Y. Fu, J. Stake, L. Dillner, M. Willander, and E. L. Kollberg, "AlGaAs/GaAs and InAlAs/InGaAs heterostructure barrier varactors," *Journal of Applied Physics*, vol. 82, no. 11, pp. 5568–5572, Dec 1997.

[11] T. A. Emadi, T. Bryllert, M. Sadeghi, J. Vukusic, and J. Stake, "Optimum barrier thickness study for the InGaAs/InAlAs/AlAs heterostructure barrier varactor diodes," *Applied Physics Letters*, vol. 90, no. 1, Jan 2007.

[12] P. J. Penfield and R. P. Rafuse, *Varactor Applications*. The M.I.T. Press.

[13] J. Stake, S. H. Jones, L. Dillner, S. Hollung, and E. L. Kollberg, "Heterostructure-Barrier-Varactor Design," *IEEE Transactions on Microwave Theory and Techniques*, vol. 48, no. 4, pp. 677–682, Apr 2000.

[14] M. Sotoodeh, A. Khalid, and A. Rezazadeh, "Empirical low-field mobility model for III-V compounds applicable in device simulation codes," *JOURNAL OF APPLIED PHYSICS*, vol. 87, no. 6, pp. 2890–2900, MAR 15 2000.

[15] M. Ingvarson, J. Vukusic, A. Olsen, T. Emadi, and J. Stake, "An electro-thermal HBV model," in *2005 IEEE MTT-S INTERNATIONAL MICROWAVE SYMPOSIUM, VOLS 1-4*, 2005, pp. 1151–1153.

[16] L. Dillner, J. Stake, and E. Kollberg, "Modeling of the heterostructure barrier varactor diode," 1997, presented at the Int. Semiconductor Device Res. Symp., Charlottesville, VA.

[17] J. Vukusic, A. Ø. Olsen, T. Bryllert, and J. Stake, "High power w-band monolithically integrated tripler," *International Conference on Infrared, Millimeter, and Terahertz Waves IRMMW 2009 Proceedings*, 2009.